Review on Chemical Stability of Lead Halide Perovskite Solar Cells

Jing Zhuang[1], Jizheng Wang[2,3], Feng Yan[1,4] ✉

HIGHLIGHTS

- A comprehensive review is presented on the chemical reactions of perovskite films underdifferent environmental conditions and with charge transfer materials and metalelectrodes in perovskite solar cells.

- The influence of chemical reactions on device stability is elucidated.

- Effective strategies for suppressing the degradation reactions are specified.

ABSTRACT Lead halide perovskite solar cells (PSCs) have become a promising next-generation photovoltaic technology due to their skyrocketed power conversion efficiency. However, the device stability issues may restrict their commercial applications, which are dominated by various chemical reactions of perovskite layers. Hence, a comprehensive illustration on the stability of perovskite films in PSCs is urgently needed. In this review article, chemical reactions of perovskite films under different environmental conditions (e.g., moisture, oxygen, light) and with charge transfer materials and metal electrodes are systematically elucidated. Effective strategies for suppressing the degradation reactions of perovskites, such as buffer layer introduction and additives engineering, are specified. Finally, conclusions and outlooks for this field are proposed. The comprehensive review will provide a guideline on the material engineering and device design for PSCs.
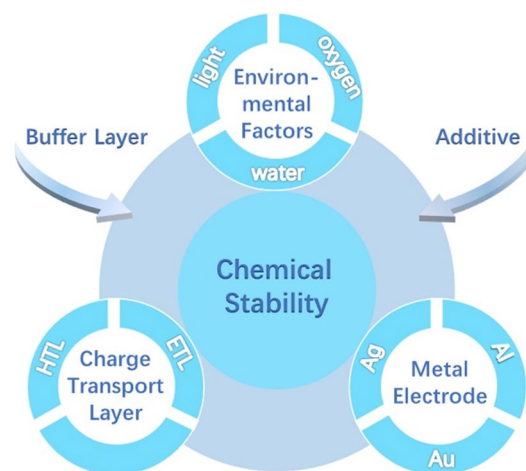
✉ Feng Yan, apafyan@polyu.edu.hk

1 Department of Applied Physics, The Hong Kong Polytechnic University, Hung Hom, Kowloon, Hong Kong SAR, People's Republic of China
2 Beijing National Laboratory for Molecular Sciences, CAS Key Laboratory of Organic Solids, Institute of Chemistry, Chinese Academy of Sciences, Beijing 100190, People's Republic of China
3 University of Chinese Academy of Sciences, Beijing 100049, People's Republic of China
4 Research Institute of Intelligent Wearable Systems, The Hong Kong Polytechnic University, Hung Hom, Kowloon, Hong Kong SAR 999077, People's Republic of China

1 Introduction

As one of the sustainable clean energy sources, photovoltaic technology has been developed vigorously in recent decades. Among them, lead halide perovskite solar cells (PSCs) stand out due to their rapidly increasing power conversion efficiency (PCE), and are currently considered as the most encouraging and promising candidate for the next generation photovoltaic technology [1–7]. In a PSC, the active light-harvesting materials are generally metal halide perovskites with a structural formula of ABX_3 (A: monovalent cation, $CH_3NH_3^+$, $HC(NH_2)_2^+$, Cs^+; B: divalent metal cation, Pb^{2+}, Sn^{2+}; X: halide anion, I^-, Br^-, Cl^-) [8–11], which are responsible for converting the incident sunlight into free carriers in the devices, therefore playing a crucial role in the conversion of energy. The extraction of free carriers depends on the electron/hole transport layers (ETL/HTL) that sandwich the perovskite layer and transport charge carriers to corresponding electrodes. Therefore, typical configurations of PSCs involve conductive glass/ETL/perovskite/HTL/electrode (n-i-p) or conductive glass/ HTL/perovskite/ ETL/electrode (p-i-n), as shown in Fig. 1 [12–16].

PSCs show advantages over commercially available solar cells in terms of low cost and little energy consumption in device fabrication. As the dominating share of the photovoltaic industry, monocrystalline silicon solar cells suffer from high fabrication cost, high-temperature preparation, bulky active layer and long payback time. In contrast, PSCs can be fabricated by solution methods at low temperature with very low fabrication cost and little material consumption [17–23]. GaAs solar cells, which have realized the highest PCE of single-junction solar
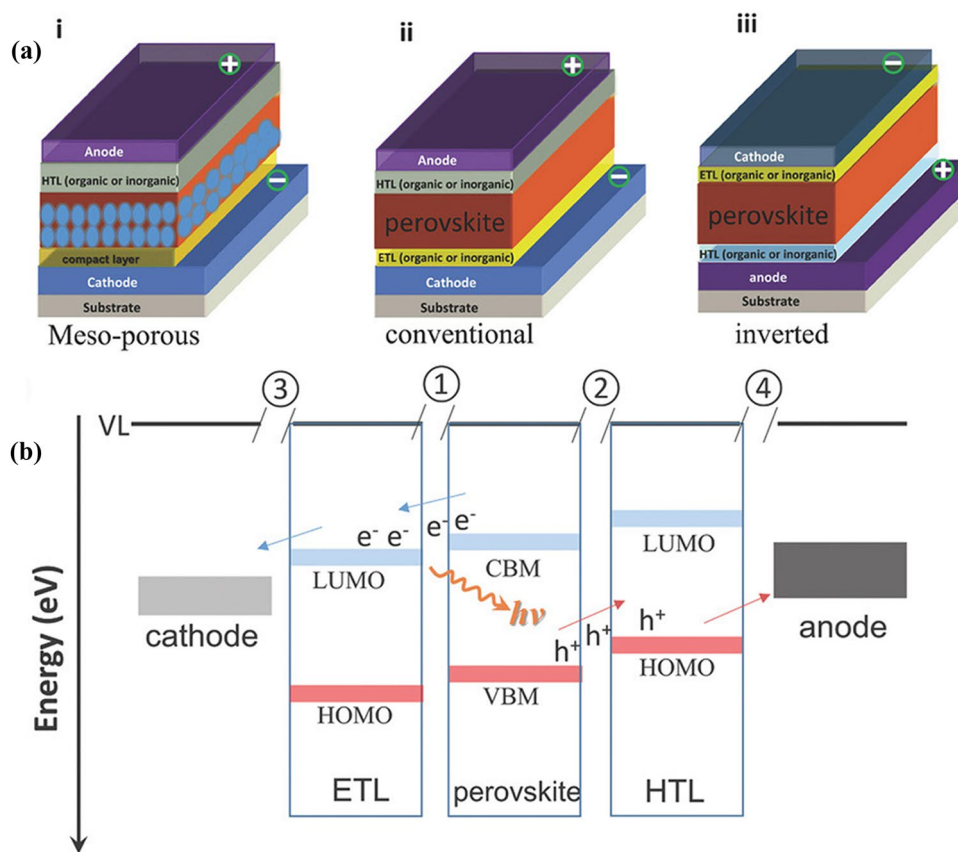

Fig. 1   a Basic structures of PSCs: (i) mesoporous structure with cathode/compact layer (TiO$_2$)/mesoporous layer (TiO$_2$ or Al$_2$O$_3$)/perovskite/ HTL/anode, (ii) conventional structure with cathode/ETL/perovskite/HTL/anode, and (iii) inverted structure with anode/HTL/ perovskite/ETL/ cathode. **b** Schematic representation of the interfaces in a planar-structured PSC. ①, ②, ③, and ④ represent ETL/perovskite interface, perovskite/HTL interface, cathode/ETL interface, and HTL/anode interface, respectively. Reproduced with permission from Ref. [12]. Copyright 2018, Wiley-VCH

cells, are only used in small-area markets such as space stations [24], while large-area PSCs (over 60 cm^2) with PCE over 20.5% have been achieved [25, 26], promising their large-area applications. Other thin film solar cells, such as copper indium diselenide (GIGS), cadmium telluride (CdTe), and quantum dot solar cells, are subject to the slow growth of efficiency [27]. Notably, the certified PCE of PSCs has exceeded 25.7% after one decade study, owing to the excellent photophysical properties of perovskites [5]. Considering the theoretical Shockley–Queisser limit of ~ 31% [28–31], there is still a relatively large space for PCE improvement for PSCs. Despite these advantages, device stability of PSCs is a critical issue to their commercial applications [32–37]. It has been recognized that device stability is closely related to a series of chemical reactions between perovskite and ETL/HTL [5, 38–40], electrodes or the environment issues (e.g., moisture, oxygen, light) [41–46].

The chemical reactions of lead halide perovskite have significant impacts on interfacial defects [47, 48], charge transport/extraction [49], and thus photovoltaic performance and device stability of PSCs [50–55]. Because of the relatively active chemical properties, perovskites may react with oxygen [56–59], water [60–63], Lewis acids and bases [64, 65] and some metals [66–70], at perovskite/charge transport layer interfaces or grain boundaries (GBs). In general, these reactions fall into two categories: 1) the reactions with species in ambient environment, including water, oxygen, and light; 2) the reactions with other materials in the device, including HTL/ETL, metal electrodes, and alternative modifiers. In order to suppress the degradation reactions of perovskites, it's necessary to reduce the reactivity of perovskites through doping additives or compositional modifications [65, 71–77]. Despite significant efforts in additive engineering, the stability of PSCs still can't meet the requirements for commercialization [78–81]. Physical isolation, another effective strategy for improving device stability, also attracts enormous attention simultaneously [82–89]. Some specific materials can serve as buffer layers to reduce the detrimental interfacial reactions. For example, the modified ZnO isolation layer with good electrical conductivity between the Ag electrode and ETL can effectively suppress the reaction between perovskite and Ag [90]. The hydrophobic diketopyrrolopyrrole-based polymers are deposited on perovskites surfaces to prevent the perovskites from being invaded by water [91]. In conclusion, understanding the chemical reactions at the interfaces can help researchers find feasible approaches to prevent the degradation of lead halide perovskites and improve the stability of PSCs.

In this review, we describe a variety of interfacial chemical reactions under different conditions, and the reactions mechanisms are also summarized. We retrospectively examined the established understanding of how the interfacial reactions affect the defects/traps formation, non-radiative recombination, ion migrations, and eventually device stability. A relatively clear relationship between device stability and interfacial chemical reactions is revealed in this part. According to different chemical reactions mechanism, we also review some available strategies for improving the chemical stability of perovskites. Finally, potential suggestions on reducing or avoiding the detrimental interfacial reactions in device fabrication and commercialization are proposed.

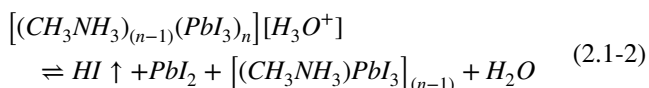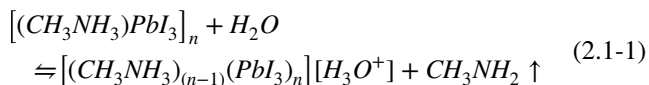# 2 Interfacial Chemical Reactions

2.1 Environmental Factors

Although encapsulated lead halide PSCs can insulate air, the challenge of achieving an ideal encapsulation effect makes it necessary to explore how environmental factors affect the chemical stability of PSCs. Both pure MAPbI$_3$ and FAPbI$_3$ are very sensitive to air due to their intrinsic instability, which can be demonstrated by their color changes from black to yellow in a few minutes, especially in high-humidity environments. Studies have shown that water and oxygen in the air can react with perovskites through different pathways. In addition, ambient light can induce the decomposition of perovskites, which will be discussed in this part.

2.1.1 Water-Induced Reactions

Many studies have revealed that the reactions of lead halide perovskites with H$_2$O can accelerate the degradation process and deteriorate the chemical stability of PSCs [60, 61, 92]. In order to express the reaction mechanism more concisely, all chemical reactions of perovskite in this review are based on the archetypal MAPbI$_3$ unless otherwise stated. Walsh et al. proposed the simple acid–base reversible reactions

between MAPbI$_3$ and H$_2$O as follows [48], and a plausible decomposition pathway for MAPbI$_3$ is shown in Fig. 2a.

$$\left[(CH_3NH_3)PbI_3\right]_n + H_2O$$
$$\leftrightharpoons \left[(CH_3NH_3)_{(n-1)}(PbI_3)_n\right][H_3O^+] + CH_3NH_2 \uparrow \quad (2.1\text{-}1)$$

$$\left[(CH_3NH_3)_{(n-1)}(PbI_3)_n\right][H_3O^+]$$
$$\rightleftharpoons HI \uparrow + PbI_2 + \left[(CH_3NH_3)PbI_3\right]_{(n-1)} + H_2O \quad (2.1\text{-}2)$$

By combining Eqs. 2.1-1 and 2.1-2, the whole degradation process of MAPbI$_3$ in the presence of H$_2$O can be generalized as follows:

$$(CH_3NH_3)PbI_3 \xrightarrow{H_2O} HI \uparrow + PbI_2 + CH_3NH_2 \uparrow \quad (2.1\text{-}3)$$
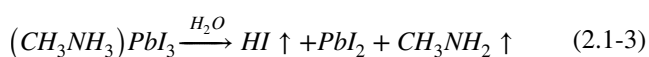
CH$_3$NH$_2$ and HI both exist in gas phases at room temperature, and thus the continuous release of gas products promotes the reaction to proceed in the forward direction.

In consequence, MAPbI$_3$ will completely degrade into PbI$_2$ once the open system contains water [93].

Wang et al. further proposed that the degradation product HI can continue to decompose into H$_2$ and I$_2$ under the stimulation of ultraviolet (UV) light [94]. The photoreaction process of HI under UV irradiation is illustrated below:

$$2HI \xrightarrow{UV} H_2 \uparrow + I_2 \quad (2.1\text{-}4)$$

The whole degradation reaction of MAPbI$_3$ when H$_2$O and UV light coexist is generalized in Eq. 2.1-5 with the combination of Eqs. 2.1-3 and 2.1-4. Therefore, the final solid products of MAPbI$_3$ decomposition are PbI$_2$ and I$_2$.

$$(CH_3NH_3)PbI_3 \xrightarrow{H_2O+UV} \frac{1}{2}H_2 \uparrow + PbI_2 + CH_3NH_2 \uparrow + \frac{1}{2}I_2 \quad (2.1\text{-}5)$$
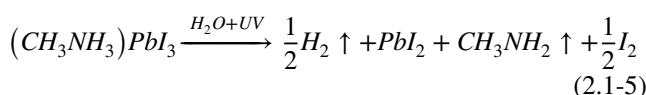
Considering that lead halide perovskites are prone to absorb H$_2$O molecule in the air to form a hydrated complex
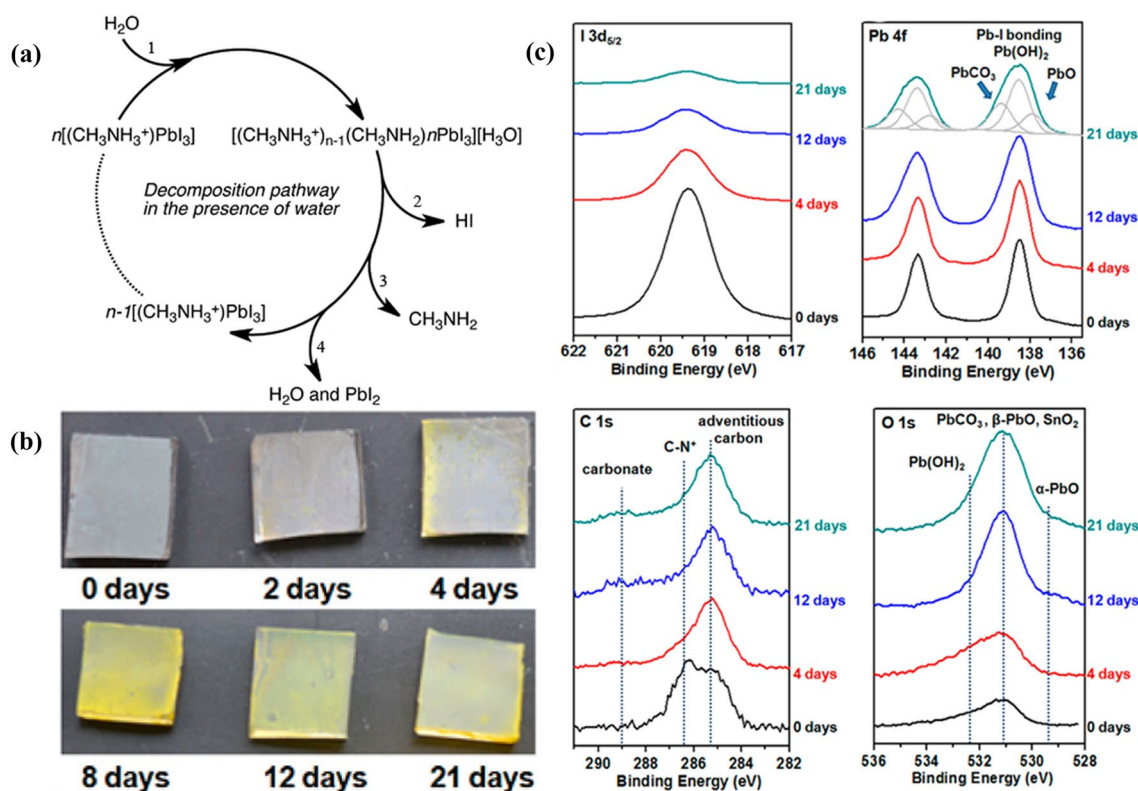
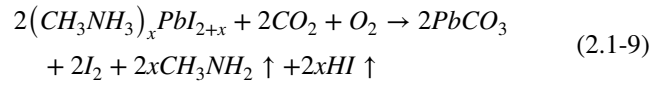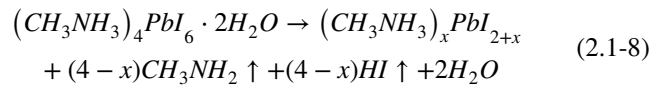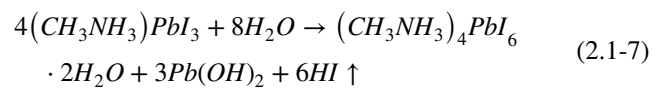**Fig. 2** **a** Possible decomposition pathway of hybrid halide perovskites in the presence of water. A water molecule, 1, is required to initiate the process with the decomposition being driven by the phase changes of both hydrogen iodide, (2, soluble in water) and the methylammonia (3, volatile and soluble in water). This pathway results in the formation of a yellow solid, which corresponds to the experimentally observed PbI$_2$, 4. Reproduced with permission from Ref. [48]. Copyright 2014, American Chemical Society. **b** Photographs of CH$_3$NH$_3$PbI$_3$ films deposited on FTO and stored under ambient conditions for several days. **c** Evolutions of photoelectron spectra of I 3d5/2, Pb 4f, C 1s and O 1s. **b**, **c** Reproduced with permission from Ref. [97]. Copyright 2016, American Chemical Society. (Color figure online)

[50, 51, 63], the hydration processes of MAPbI$_3$ are displayed in Eqs. 2.1-6 and 2.1-7, respectively. Notably, the decoloring process of black perovskites induced by the generation of monohydrated phase CH$_3$NH$_3$PbI$_3\cdot$H$_2$O is reversible [95], and that can be reconverted into MAPbI$_3$ again through dehydration process [63]. However, the degradation reactions become irreversible once the dihydrate (CH$_3$NH$_3$)$_4$PbI$_6\cdot$2H$_2$O forms (Eq. 2.1-7). Here, in the hydration process, the [PbI$_6$]$^{4-}$ in the 3D network of MAPbI$_3$ decays to a 0D framework of isolated octahedral. Ptasinska et al. pointed out that a transient phase PbI$_{2+x}{}^{x-}$ ($0 \leq \text{x} < 1$) forms during the evolution of a hydrated complex under ambient conditions [96]. The resulting PbI$_{2+x}{}^{x-}$ is reactive when exposed to air and decomposes into lead-containing compounds inducing amorphous PbO, Pb(OH)$_2$, and PbCO$_3$ (Eqs. 2.1-9, 2.1-10, 2.1-11), which is evidenced by X-ray photoelectron spectra (XPS) characterizations in Fig. 2c.

$$(CH_3NH_3)PbI_3 + H_2O \rightleftharpoons (CH_3NH_3)PbI_3 \cdot H_2O \quad (2.1\text{-}6)$$

$$4(CH_3NH_3)PbI_3 + 8H_2O \rightarrow (CH_3NH_3)_4 PbI_6 \\ \cdot 2H_2O + 3Pb(OH)_2 + 6HI \uparrow \quad (2.1\text{-}7)$$

$$(CH_3NH_3)_4 PbI_6 \cdot 2H_2O \rightarrow (CH_3NH_3)_x PbI_{2+x} \\ + (4-x)CH_3NH_2 \uparrow + (4-x)HI \uparrow + 2H_2O \quad (2.1\text{-}8)$$

$$2(CH_3NH_3)_x PbI_{2+x} + 2CO_2 + O_2 \rightarrow 2PbCO_3 \\ + 2I_2 + 2xCH_3NH_2 \uparrow + 2xHI \uparrow \quad (2.1\text{-}9)$$

$$(CH_3NH_3)_x PbI_{2+x} + H_2O + \frac{1}{2}O_2 \rightarrow Pb(OH)_2 \\ + I_2 + xCH_3NH_2 \uparrow + xHI \uparrow \quad (2.1\text{-}10)$$

$$Pb(OH)_2 \rightarrow PbO + H_2O \quad (2.1\text{-}11)$$
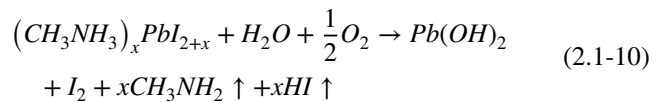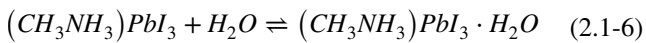
It's reported that trapped charges can facilitate the degradation reactions of MAPbI$_3$ in humid conditions. Ahn et al. deposited different polarity ions on the perovskite surfaces in humidified nitrogen and discovered that MAPbI$_3$ is irreversibly decomposed to yellow PbI$_2$ only when moisture and charges coexist (Fig. 3a–d) [97]. Figure 3e–l demonstrate
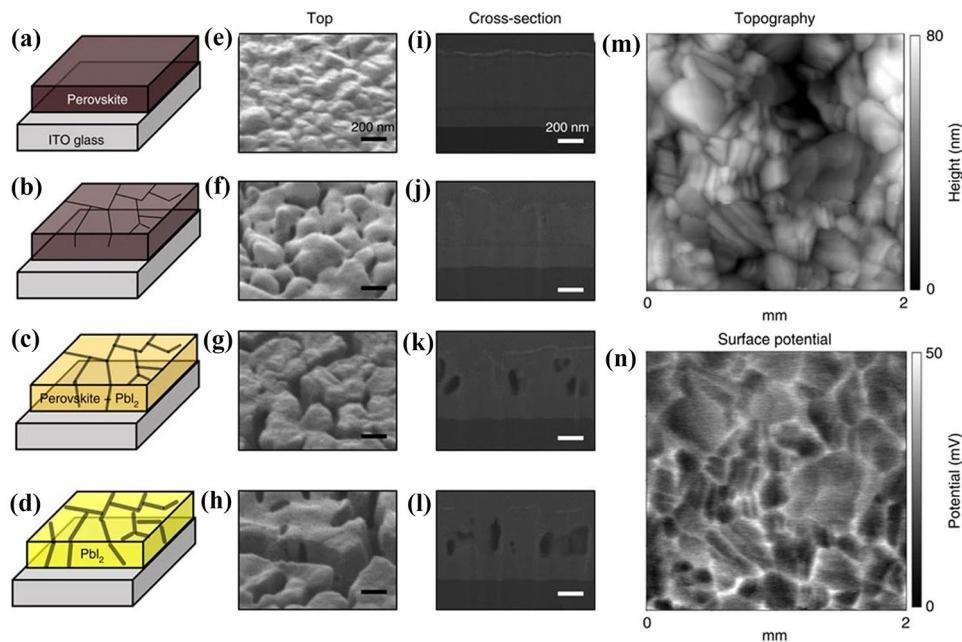

Fig. 3 **a–d** Schematic illustration of perovskite degradation processes (left), **e–h** top-view (middle) and **i–l** cross-sectional (right) SEM images of perovskite layers (**a, e, i**) before, (**b, f, j**) after 6 h, (**c, g, k**) 12 h and (**d, h, l**) 18 h by ion deposition in humidified nitrogen. The color change from dark brown to yellow in **a-d** represents the gradual degradation process. Black lines and their widths in **a–d** represent grain boundaries and degradation extent, respectively. Scale bars, 200 nm. **m** Topography and **n** surface potential profile of MA$_{0.6}$FA$_{0.4}$PbI$_{2.9}$Br$_{0.1}$ film obtained from KPFM measurements after deposition of N$_2$-positive ions. Reproduced with permission from Ref. [98]. Copyright 2016, Springer Nature. (Color figure online)

that the degradation of perovskite starts from the GBs and the striking resemblance in kelvin probe force microscopy (KPFM) measurements (Fig. 3m and n) indicates that charges are preferentially trapped along GBs, which demonstrates that trapped charges can give rise to irreversible degradation. The degradation mechanism can be summarized: first, the perovskite material undergoes a hydration reaction in humid environment. Next, the organic cations, like MA$^+$, will be deprotonated with the help of the local electric field induced by the charges trapped at the defect sites. The deprotonation process in the presence of water is shown below:

$$CH_3NH_3^+ + H_2O \xrightarrow{TC} CH_3NH_2 \uparrow + H_3O^+ \tag{2.1-12}$$
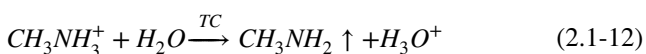
Here TC represents trapped charges. The release of gas phase CH_3NH_2 will shift the following hydration equilibrium reaction to the right side, causing the perovskite to start irreversible decomposition:

$$(CH_3NH_3)PbI_3 + H_2O \xrightarrow{TC} PbI_2 + CH_3NH_2 \uparrow + H_3O^+ + I^- \tag{2.1-13}$$
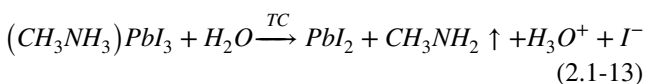
In addition, oxygen can also accelerate the aging of perovskite in humid conditions, which is attributed to the scavenging action of O_2 on the H_3O^+ proton formed in the aforementioned deprotonation process (Eq. 2.1-12). The overall degradation reaction of MAPbI$_3$ with the participation of O_2 is shown as follows:
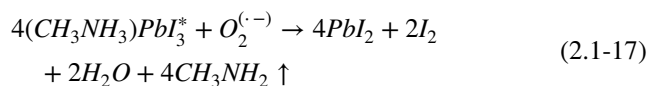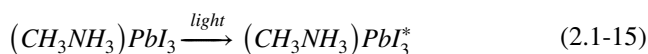
$$(CH_3NH_3)PbI_3 + \frac{1}{4}O_2 \xrightarrow{H_2O+TC} PbI_2 + CH_3NH_2 \uparrow + \frac{1}{2}H_2O + \frac{1}{2}I_2 \tag{2.1-14}$$
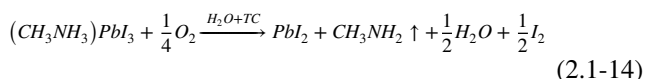
In summary, lead halide perovskite can easily decompose into PbI$_2$, CH$_3$NH$_2$, HI, and other products in humid conditions with/without other factors (e.g. UV light, trapped charges, oxygen). The degradation reaction of MAPbI$_3$ is usually irreversible due to the formed gas products (e.g. CH$_3$NH$_2$, HI) will release into the air. Therefore, protecting perovskites from water is crucial to improve the stability of PSCs.
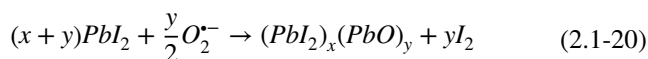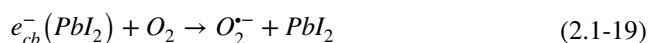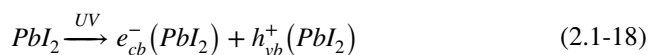
2.1.2 Oxygen-Induced Reactions

Oxygen can induce the degradation of lead halide perovskites under certain conditions [98]. A study found that O_2 molecules are only physically attached to the perovskites surfaces without chemical reactions. Once the adsorbed O_2 captures an excess electron to form superoxide ($O_2^{\cdot-}$), the degradation reactions of perovskites will proceed [99].

Haque et al. reported that O_2 could permeate into the grain surface and interior of MAPbI$_3$, which could also be reduced to highly reactive $O_2^{\cdot-}$ with the help of photo-excited electrons [57, 100]. It's observed that the Al$_2$O$_3$/MAPbI$_3$ system can produce more $O_2^{\cdot-}$ than TiO$_2$/MAPbI$_3$ system. In Fig. 4a, the TiO$_2$ film can accept an electron from the photo-excited MAPbI$_3$ because of the favorable energy offset at the heterojunction. Therefore, the fewer electrons transferring to oxygen leads to a lower yield of $O_2^{\cdot-}$ for the TiO$_2$/MAPbI$_3$ system. Simultaneously, ab initio simulations demonstrate the $O_2^{\cdot-}$ prefer energetically to occupy the iodide vacancies sites [101]. The photo-induced $O_2^{\cdot-}$ formation is the key factor for the degradation reactions of MAPbI$_3$:

$$(CH_3NH_3)PbI_3 \xrightarrow{light} (CH_3NH_3)PbI_3^* \tag{2.1-15}$$

$$O_2 \xrightarrow{(CH_3NH_3)PbI_3^*} O_2^{\cdot-} \tag{2.1-16}$$

$$4(CH_3NH_3)PbI_3^* + O_2^{(\cdot-)} \rightarrow 4PbI_2 + 2I_2 + 2H_2O + 4CH_3NH_2 \uparrow \tag{2.1-17}$$

CH$_3$NH$_3$PbI$_3^*$ carries both photo-induced electrons and holes (Eq. 2.1-15), and O_2 captures an electron from CH$_3$NH$_3$PbI$_3^*$ to form $O_2^{\cdot-}$ (Eq. 2.1-16). The study found that MAPbI$_3$ films with large grains degrade more slowly, which is attributed to large crystallites containing the fewer surface reaction sites. Based on the studies above, Sultana et al. discovered that the degradation product PbI$_2$ (Eq. 2.1-17) could further react with O_2 to produce lead oxyiodide under UV irradiation [38], which can be expressed as follows:

$$PbI_2 \xrightarrow{UV} e_{cb}^-(PbI_2) + h_{vb}^+(PbI_2) \tag{2.1-18}$$

$$e_{cb}^-(PbI_2) + O_2 \rightarrow O_2^{\cdot-} + PbI_2 \tag{2.1-19}$$

$$(x + y)PbI_2 + \frac{y}{2}O_2^{\cdot-} \rightarrow (PbI_2)_x(PbO)_y + yI_2 \tag{2.1-20}$$

The electron is excited from the valence band of PbI$_2$ to its conduction band under UV irradiation (Eq. 2.1-18), which then transfers to O_2 molecular to generate $O_2^{\cdot-}$ (Eq. 2.1-19). Finally, the highly reactive $O_2^{\cdot-}$ further reacts with PbI$_2$ generating lead oxyiodide.

It's reported that $O_2^{\cdot-}$ will capture an acid proton of the CH$_3$NH$_3^+$ to generate hydroperoxyl radical (HO$_2\cdot$) once approaching the ammonium group (Eq. 2.1-21) [102, 103].
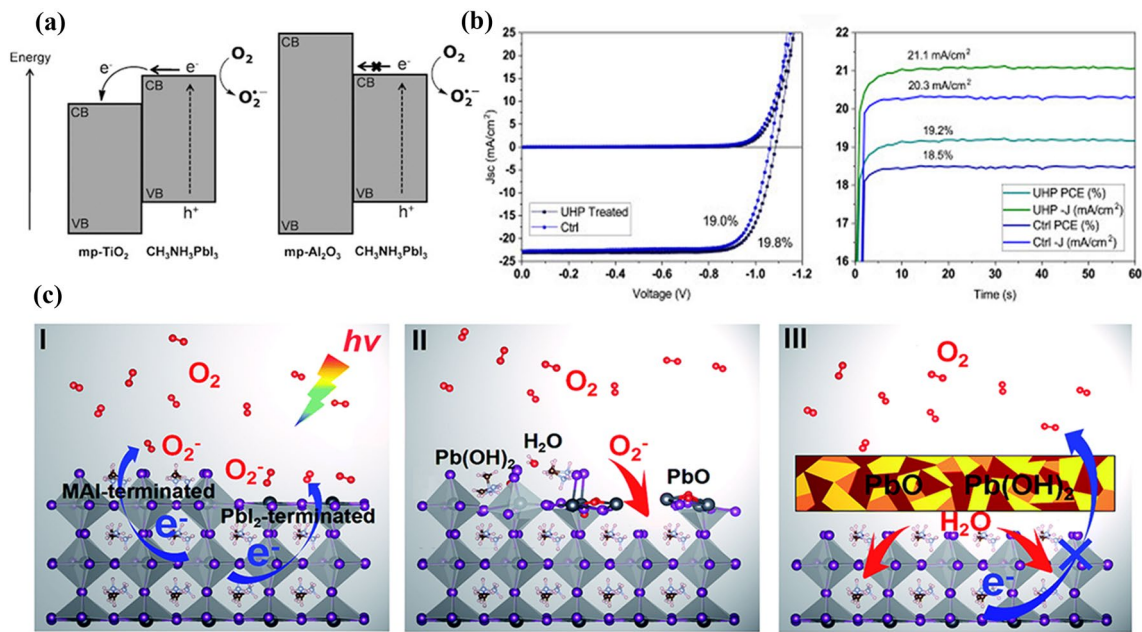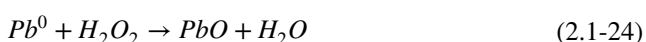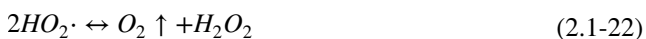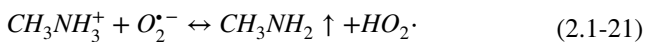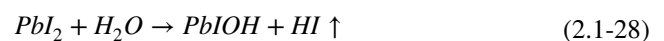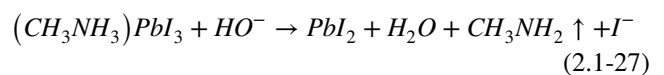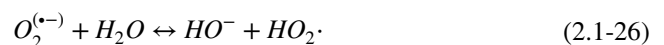
Fig. 4 **a** Schematic model showing the electron transfer of the photoexcited electrons in the MAPbI$_3$ layers to oxygen resulting in the formation of superoxide. Reproduced with permission from Ref. [101]. Copyright 2015, Wiley-VCH. **b** Photovoltaic performance characteristics of p-i-n PSC treated by H$_2$O$_2$ via the gas-phase deposition method with urea hydrogen peroxide for 40 s, compared to a control device, measured under AM1.5 100 mW/cm^2 simulated sunlight. Reproduced with permission from Ref. [103]. Copyright 2019, Elsevier. **c** Schematic representation of the photo-oxidative degradation process of the MAPbI$_3$ (001) surface. Reproduced with permission from Ref. [108]. Copyright 2019, Royal Society of Chemistry

Subsequently, two different reaction mechanisms are proposed to express next degradation process of perovskite. The first one is that two HO$_2$· interact to produce hydrogen peroxide (H$_2$O$_2$) under lights (Eq. 2.1-22). Ultimately, H$_2$O$_2$ reacts with Pb^0 on the perovskite surface generating PbO or Pb(OH)$_2$ (Eqs. 2.1-23, 2.1-24). It is worth noting that the formed PbO has an unexpected passivation effect, preventing the accumulation of anion vacancies and formation of Pb-Pb dimers, which can increase the open-circuit voltage (V_{oc}) for inverted PSCs as exhibited in Fig. 4b. The second one demonstrates that HO$_2$· radicals can dissociate into H$_2$ and O$_2$, and the remaining O$_2$ can serve as a reactant again for the continuous degradation process (Eq. 2.1-25).

$$CH_3NH_3^+ + O_2^{\bullet -} \leftrightarrow CH_3NH_2 \uparrow + HO_2 \cdot \qquad (2.1\text{-}21)$$

$$2HO_2 \cdot \leftrightarrow O_2 \uparrow + H_2O_2 \qquad (2.1\text{-}22)$$

$$Pb^0 + H_2O_2 \rightarrow Pb(OH)_2 \qquad (2.1\text{-}23)$$

$$Pb^0 + H_2O_2 \rightarrow PbO + H_2O \qquad (2.1\text{-}24)$$

$$2HO_2 \cdot \leftrightarrow 2O_2 \uparrow + H_2 \uparrow \qquad (2.1\text{-}25)$$

Hillhouse et al. reported that H$_2$O can accelerate the photooxidation reaction of MAPbI$_3$ and proposed one plausible degradation pathway [104]. H$_2$O rapidly undergoes the deprotonation reaction to form HO$_2$· and HO$^-$ in the presence of O$_2$·$^-$ (Eq. 2.1-26). As mentioned above, the newly formed HO$_2$· will interact to release H$_2$ and O$_2$ (Eq. 2.1-25). Unfortunately, HO$^-$ triggers the decomposition of MAPbI$_3$ into PbI$_2$ (Eq. 2.1-27), which subsequently reacts with H$_2$O to generate PbIOH and HI (Eq. 2.1-28) in the following steps:

$$O_2^{(\bullet -)} + H_2O \leftrightarrow HO^- + HO_2 \cdot \qquad (2.1\text{-}26)$$

$$\left(CH_3NH_3\right)PbI_3 + HO^- \rightarrow PbI_2 + H_2O + CH_3NH_2 \uparrow + I^- \qquad (2.1\text{-}27)$$

$$PbI_2 + H_2O \rightarrow PbIOH + HI \uparrow \qquad (2.1\text{-}28)$$

It's worth noting that O$_2$·$^-$ more rapidly reacts with H$_2$O (Eq. 2.1-26) than CH$_3$NH$_3^+$ (Eq. 2.1-21) due to a lower activation energy for the whole reaction pathway, which

demonstrates that H_2O can accelerate photooxidative degradation of MAPbI$_3$.

Except for the degradation products mentioned above like PbI$_2$ and lead oxyiodide, Snaith et al. detected metal lead (Pb^0) on the perovskite surface [105] and proposed a plausible formation mechanism of Pb^0 [102]. An iodide ion (I$^-$) abstracts a photogenerated hole (h$^+$) to produce an iodine atom (I$^\bullet$) (Eq. 2.1-29), which is accompanied by rapid site exchange of iodide from a regular to interstitial lattice site. Two iodine atoms combine with each other to generate I$_2$, simultaneously leaving two iodine vacancies (V$_I$) (Eq. 2.1-30). Subsequently, V$_I$ captures an electron to generate Farbe center (V$_I$e') (Eq. 2.1-31), which then reduces the Pb^{2+} in the adjacent site to Pb$^+$ (Eq. 2.1-32). Finally, Pb$^+$ undergoes a disproportionation reaction to produce Pb^0 (Eq. 2.1-33).

$$I^- + h^+ \rightarrow I^\bullet \tag{2.1-29}$$

$$2I^\bullet \rightarrow I_2 + 2V_{I^\bullet} \tag{2.1-30}$$

$$V_{I^\bullet} + e^{'} \rightarrow V_{I^\bullet}e^{'} \tag{2.1-31}$$

$$Pb^{2+} + V_{I^\bullet}e^{'} \rightarrow V_{I^\bullet}Pb^+ \tag{2.1-32}$$
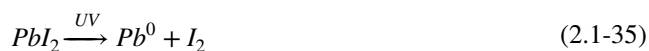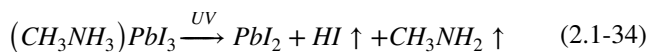
$$2Pb^+ \rightarrow Pb^{2+} + Pb^0 \tag{2.1-33}$$

Based on the above research, a photo-oxidative degradation mechanism of MAPbI$_3$ is proposed for rapid surface oxidation and slow inner hydration [101, 106]. Wang et al. reported the three-step degradation process of MAPbI$_3$ as displayed in Fig. 4c [107]. Step I: O$_2$ on the MAPbI$_3$ surface capture a photogenerated electron from the conduction band of MAPbI$_3$ to form O$_2^-$ (Eq. 2.1-16). Step II: O$_2^-$ rapidly oxidizes the PbI$_2$-terminated surface to produce PbO, resulting in a breakage of the Pb–I frameworks and the exposure of the MAI-terminated surface. Subsequently, the underlying MAI-terminated surface is further oxidized to generate H$_2$O and PbO or the unstable Pb(OH)$_2$. Step III: The oxidation products PbO and Pb(OH)$_2$ can act as protective layers to inhibit the further oxidation of the internal MAPbI$_3$. The newly produced H$_2$O molecules from the surface oxidation and decomposition of Pb(OH)$_2$ can slowly hydrate with the internal MAPbI$_3$, finally leading to the structural collapse of MAPbI$_3$.

In conclusion, the oxygen-induced reactions of perovskites need the participation of light or water. Firstly, O$_2$ captures photogenerated electrons generating O$_2^-$, which subsequently introduces a series of decomposition pathways under different conditions. Finally, the generating degradation products mainly include CH$_3$NH$_2$, I$_2$, PbI$_2$, and PbO (or Pb(OH)$_2$).

2.1.3 Light-Induced Reactions

Unlike oxygen, light can induce the perovskites degradation without any presence of other environmental factors (e.g., water, oxygen). Study demonstrated that UV light can induce severe degradation of lead halide perovskites [108, 109]. As shown in Fig. 5a, Gao et al. detected Pb^0 on the MAPbI$_3$ surface after about 120 min of UV irradiation with a wavelength of 408 nm [110]. The proposed degradation reactions of MAPbI$_3$ under UV irradiation can be generalized in Eqs. 2.1-34, 2.1-35. Figure 5b shows that the ratio of Pb^0 remains nearly constant after 480 min of UV irradiation, which indicates that the decomposition of MAPbI$_3$ has already saturated.

$$\left(CH_3NH_3\right)PbI_3 \xrightarrow{UV} PbI_2 + HI \uparrow + CH_3NH_2 \uparrow \tag{2.1-34}$$

$$PbI_2 \xrightarrow{UV} Pb^0 + I_2 \tag{2.1-35}$$

Yan et al. proposed a possible photodegradation mechanism of MAPbI$_3$ concerning hot carriers [111]. As shown in Fig. 5c, the first step is that MAPbI$_3$ is excited by light ($hv > 3$ eV) to generate long-lived hot carriers (Eq. 2.1-36). Then a hot electron reacts with the CH$_3$NH$_3^+$ via columbic coupling to generate a free proton and release CH$_3$NH$_2$ near surface or GB regions (Eq. 2.1-37). Finally, the free protons interact with undercoordinated I$^-$ on the surface, generating volatile HI and iodine vacancies (Eq. 2.1-38). The release of HI can induce the destruction of Pb-I framework from the corner-shared to the face-shared Pb-I octahedral, causing the degradation of MAPbI$_3$ into PbI$_2$.

$$hv(> 3\text{eV}) \rightarrow e^-(hot) + h^+(hot) \tag{2.1-36}$$

$$CH_3NH_3^+ + e^-(hot) \rightarrow CH_3NH_2 + H^+ + e^- \tag{2.1-37}$$

$$I^- + H^+ \rightarrow HI \uparrow + V_I \tag{2.1-38}$$

It's reported that halide defects have an influence on the photostability of MAPbI$_3$ [112]. Petrozza et al. found
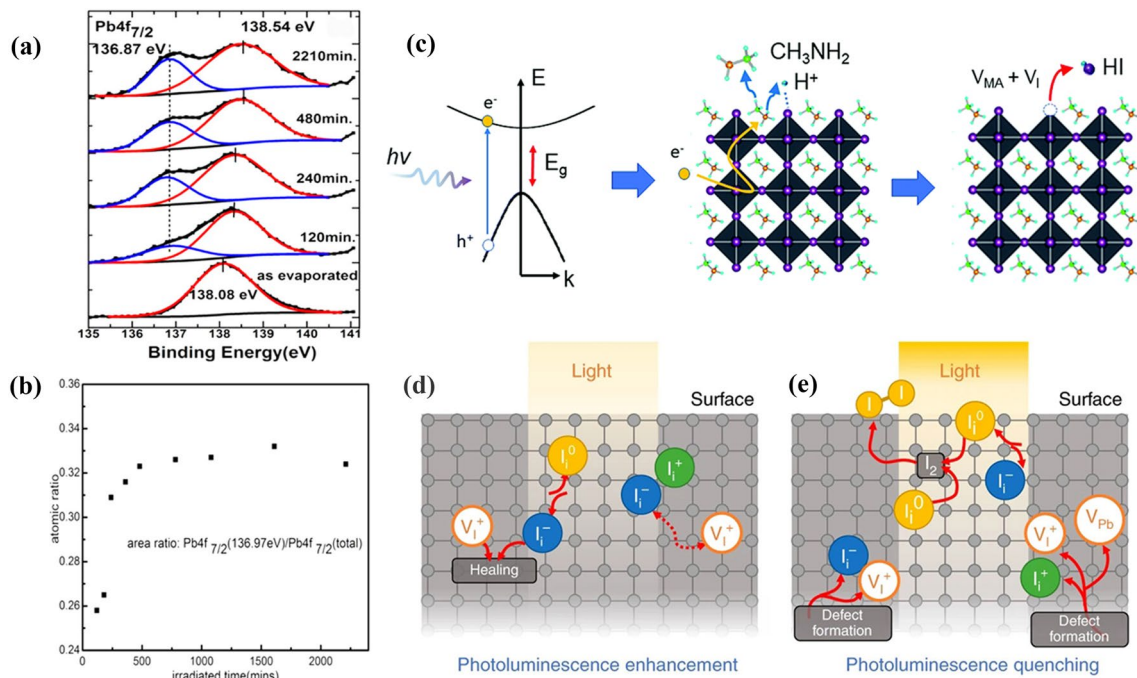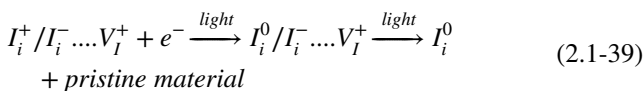
Fig. 5 **a** Pb 4f7/2 decomposition and **b** metallic Pb fraction during laser irradiation. **a**, **b** Reproduced with permission from Ref. [111]. Copyright 2017, American Chemical Society. **c** Schematic representation of photodegradation mechanism. 1) Hot carrier generation, 2) deprotonation and release of MA gas, and 3) formation of HI gas and V_I. Reproduced with permission from Ref. [112]. Copyright 2018, Royal Society of Chemistry. **d**, **e**, Photoluminescence enhancement and quenching mechanisms. Ion dynamics in MAPbI$_3$ thin film promoting PLIE in **d**, when the probability of I$_0$ species encounters is small and Frenkel pair annihilation is boosted by electron trapping, and PLID in **e**, when the probability of I$_0$ species encounters is high, boosting I$_2$ molecule formation. **d**, **e** Reproduced with permission from Ref. [113]. Copyright 2019, Springer Nature

that long-living carrier traps associated with halide defects could trigger photoconversion, which drives both photoluminescence intensity enhancement (PLIE) and photoluminescence intensity decrease (PLID). In Fig. 5d and e, PLIE and PLID processes are proposed to explain the observations. The timescales involved in PLID and PLIE are consistent with the reported ionic activities, such as ion/defect annihilation and migration rates [113, 114]. Generally, vacancies (e.g., V_{Pb}) and interstitial halogen (e.g., I_i) defects dominate in the perovskites. V_{Pb} is only moderately active as a trap, while I_i can remarkably trap both electrons and holes via $(+/0)$ and $(0/-)$ transitions. When the probability of encountering I^0 species is very low, the light-induced PLIE is associated with annihilation of the $I_i^- V_I^+$ Frenkel pair:

$$I_i^+/I_i^- .... V_I^+ + e^- \xrightarrow{light} I_i^0/I_i^- .... V_I^+ \xrightarrow{light} I_i^0$$
$$+ \, pristine \, material$$

(2.1-39)

The PLID mechanism is proposed to be a bimolecular reaction boosted by increasing the encountering probability of I^0 species, occurring near the film surface filled with long-lived traps:

$$2I_i^0 \xrightarrow{light} I_2$$

(2.1-40)

The two processes may coexist and compete in the perovskite material. If traps densities are adequately low, photo-induced PLIE will be a dominant effect. However, photo-induced PLID will play a key role when high-density traps appear near the film surface that may act as a reservoir for photogenerated species, eventually causing perovskites degradation. Therefore, passivating under-coordinated surface sites can prohibit defect formation and hence enhance the photostability of perovskites.

2.2 Charge Transport Layers

In addition to the aforementioned degradation reactions induced by environmental factors, the chemical stability of lead halide PSCs can be affected by charge transport layers, including ETL and HTL. Generally, the interfacial chemical reactions are not desirable, which could lead to destroyed structure and reduced charge transport/extraction. However, for certain charge transport layers such as Cl-containing SnO$_2$, interfacial reactions have been demonstrated to be beneficial for charge transport and chemical stability of PSCs. Considering the diversity of charge transport materials, a variety of interfacial reactions and their effects on device stability have been reported in literature. Therefore,

the chemical reactions in PSCs induced by charge transport layers are elucidated in this session.

2.2.1 ETL-Induced Reactions

TiO$_2$ has been widely used as an electron transport material in the early study of PSCs [36, 115–121]. Belmonte et al. reported that TiO$_2$ interacts with MAPbI$_3$ mainly through binding I$^-$ in MAPbI$_3$ to undercoordinated Ti^{4+} in TiO$_2$ [49, 122]. Notably, this Ti-I-Pb bond is not strong due to the little hybridization between Pb$_{s-p}$ state and Ti$_d$ orbital, hence the adsorption/desorption of I$^-$ at the interface may occur easily. The interactions between TiO$_2$ and perovskite are reversible under both positive and negative biases, as shown in Fig. 6a–c. At a positive bias, weakly bonded I$^-$ migrate
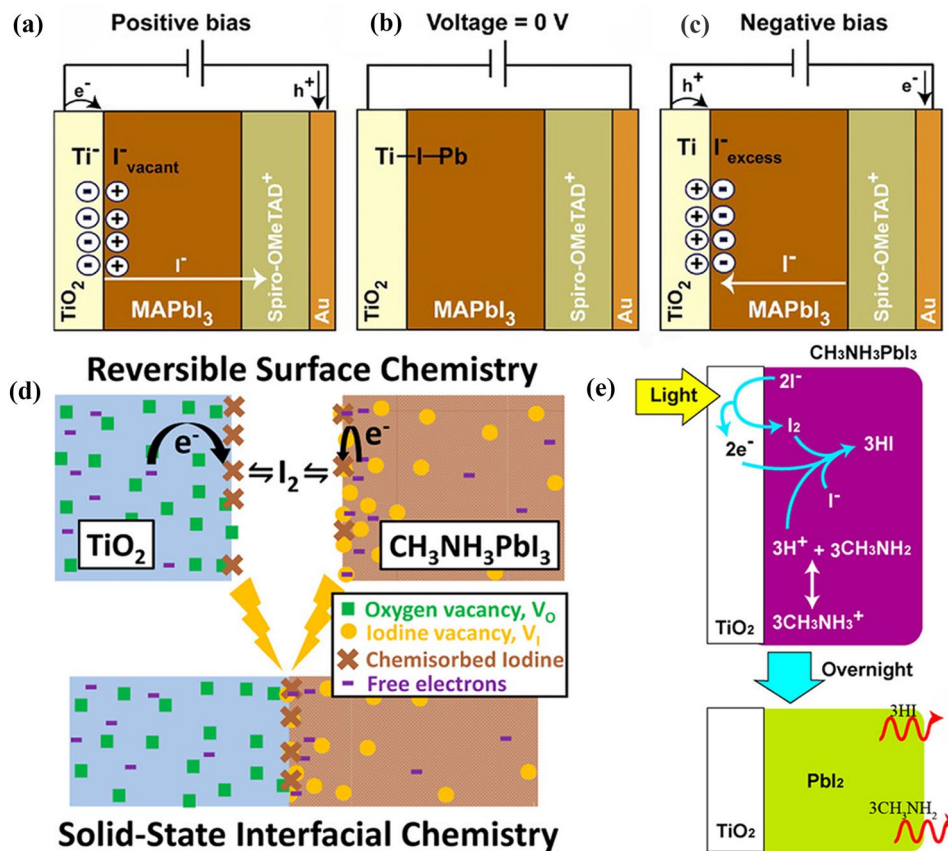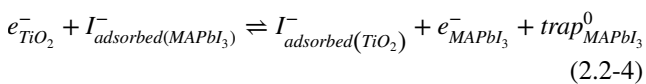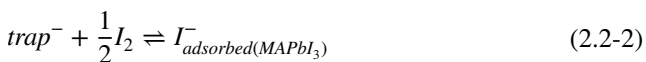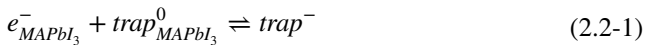

Fig. 6 Diagram representing iodide migration and chemical species present at the interfaces. **a** At positive-bias iodine ions are forced to migrate toward the hole selective contact where the reaction with spiro-OMeTAD$^+$ occurs. The iodide defective layer is formed at the TiO$_2$/MAPbI$_3$ interface. **b** At zero-bias the neutral case appears. **c** At negative-bias spiro-OMeTAD only partially returns to its oxidized, conductive state. Iodide ions accumulate at the TiO$_2$/perovskite interface. **a-c** Reproduced with permission from Ref. [49]. Copyright 2016, Wiley-VCH. **d** Scheme showing the reversible chemistry reactions process occurring at the solid-state TiO$_2$/CH$_3$NH$_3$PbI$_3$ interface. Reproduced with permission from Ref. [124]. Copyright 2017, American Chemical Society. **e** Degradation scheme of CH$_3$NH$_3$PbI$_3$ perovskite solar cells during light exposure test: TiO$_2$/CH$_3$NH$_3$PbI$_3$. Reproduced with permission from Ref. [125]. Copyright 2014, American Chemical Society

towards the hole transport layer contact and hence I vacancies remain at MAPbI$_3$/TiO$_2$ interface, and the positive charges are compensated by electrons injection and accumulations at TiO$_2$. In contrast, excess I$^-$ may accumulate at MAPbI$_3$/TiO$_2$ interface under a negative bias. The Ti-I-Pb bonds easily accommodate excessive defect or ion charges in a highly reversible manner to generate capacitive currents. However, it's worth noting that this reversible interaction has a negligible effect on the photovoltaic performance and chemical stability of PSCs.

Studies on film's current response to I$_2$ vapor have revealed that reversible chemical reactions occur at TiO2/I$_2$ and MAPbI3/I$_2$ interfaces [123]. Rand et al. discovered the pathways for I$_2$ passivation of MAPbI$_3$ surface defects from the photoconductivity data of MAPbI$_3$ films. According to the current response of TiO$_2$ film to I$_2$ vapor pressures, they proposed a plausible reaction mechanism between TiO$_2$ and I$_2$. As shown in Eqs. 2.2-1, 2.2-2, and 2.2-3, TiO$_2$ and MAPbI$_3$ surfaces undergo strong reversible reactions with I$_2$ gas, respectively. Combining these three reactions, the chemical interaction between TiO$_2$ and MAPbI$_3$ can be generalized in Eq. 2.2-4.

$$e^-_{MAPbI_3} + trap^0_{MAPbI_3} \rightleftharpoons trap^- \tag{2.2-1}$$

$$trap^- + \frac{1}{2}I_2 \rightleftharpoons I^-_{adsorbed(MAPbI_3)} \tag{2.2-2}$$

$$e^-_{TiO_2} + \frac{1}{2}I_2 \rightleftharpoons I^-_{adsorbed(TiO_2)} \tag{2.2-3}$$

$$e^-_{TiO_2} + I^-_{adsorbed(MAPbI_3)} \rightleftharpoons I^-_{adsorbed(TiO_2)} + e^-_{MAPbI_3} + trap^0_{MAPbI_3} \tag{2.2-4}$$

I$^-$ in MAPbI$_3$ is adsorbed on the TiO$_2$ surface and deplete an electron on TiO$_2$, leaving a free electron as well as a trap on the MAPbI$_3$ surface (Fig. 6d). The energy level of the trap would determine whether the electron is captured or freely transmitted. Therefore, MAPbI$_3$ may be chemically reduced by TiO$_2$ due to the differences in work function. In addition, the newly formed traps on the MAPbI$_3$ surface will make a difference to carrier density and recombination rate, which could deteriorate the device stability.

TiO$_2$ was also reported to catalyze MAPbI$_3$ decomposition in the presence of light [124]. In Fig. 6e, TiO$_2$ extracts an electron from I$^-$ under light irradiation generating I$_2$ (Eq. 2.2-5), which deconstructs perovskites crystal and reduces their chemical stability. As mentioned in *2.2.1* part,

CH$_3$NH$_3^+$ can be deprotonated to generate CH$_3$NH$_2$ and H$^+$ in humid conditions. The presence of I$_2$ and H$^+$ will accelerate the reaction (Eq. 2.2-6) to proceed forward, further destroying the perovskite structure.

$$2I^- \xrightarrow{TiO_2+light} I_2 + 2e^-_{TiO_2} \tag{2.2-5}$$

$$I^- + I_2 + 3H^+ + 2e^-_{TiO_2} \rightleftharpoons 3HI \uparrow \tag{2.2-6}$$

TiO$_2$ acts as a catalyzer rather than a reagent in the reactions with perovskites, which accelerates the degradation process of perovskites to some extent. Therefore, reducing the catalytic performance of TiO$_2$ is an effective way to improve the photovoltaic performance and chemical stability of TiO$_2$-based PSCs.

It's reported that ZnO ETL can also interact chemically with perovskites [125–129]. Anta et al. proposed that an acid–base reaction could occur at the ZnO/perovskite interface [130], triggering the decomposition of perovskite into PbI$_2$ in humid conditions. In addition, this interaction could cause redissolution of the ZnO substrate, whose morphology changes from spherical nanoparticles to aciculate particles (Fig. 7a).

Additionally, the deprotonation reaction between ZnO and perovskite can cause the thermal degradation of perovskite. Kelly et al. found that the basic hydroxyl groups and residual acetate ligands exist on the ZnO surface through the Fourier transform infrared spectroscopy (FTIR) spectra analysis (Fig. 7b), which can be eliminated or reduced by high-temperature calcination of ZnO films (Fig. 7c) [131]. Otherwise, the hydroxide or residual acetate ligands will react with CH$_3$NH$_3^+$ destroying the crystal structure of perovskite, which is evidenced in Fig. 7d and e [132]. And this decomposition process of MAPbI$_3$ can be expressed as follows:

$$OH^- + CH_3NH_3^+ \rightarrow CH_3NH_3OH \tag{2.2-7}$$

$$CH_3NH_3OH \xrightarrow{heat} CH_3NH_2 \uparrow + H_2O \tag{2.2-8}$$
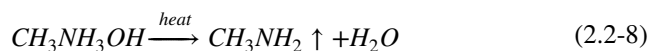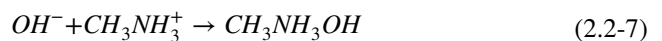
As shown in Eqs. 2.2-7 and 2.2-8, the whole degradation reactions are the deprotonation process of CH$_3$NH$_3^+$, and CH$_3$NH$_3$OH easily decomposes into CH$_3$NH$_2$ gas and H$_2$O under heat. The decomposition of CH$_3$NH$_3$OH can promote the reaction (Eq. 2.2-7) to proceed forward continuously, which accelerates MAPbI$_3$ degradation. It's reported that MAPbI$_3$ decomposes easily to form HI in humid conditions [94], which subsequently reacts with ZnO resulting in
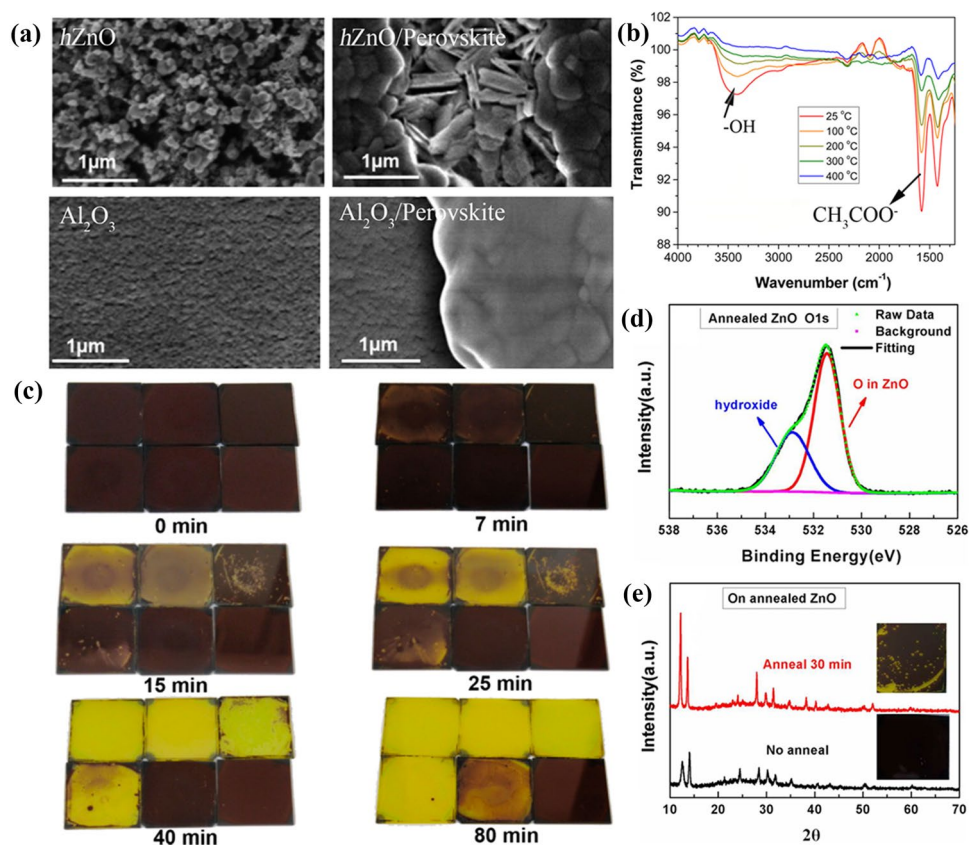
Fig. 7 **a** SEM of *h*ZnO and Al$_2$O$_3$ substrates before (left) and after (right) deposition of perovskite layer. Reproduced with permission from Ref. [131]. Copyright 2016, Royal Society of Chemistry. **b** FTIR spectra of ZnO films on glass annealed at various temperatures. **c** Photographs of CH$_3$NH$_3$PbI$_3$ films deposited on thermally pretreated ZnO layers and heated to 100 °C for the indicated time: top row (left to right): pretreated at 25, 100, 200 °C. Bottom row (left to right): pretreated at 300 °C, 400 °C, and SiO$_2$/CH$_3$NH$_3$PbI$_3$. **b, c** Reproduced with permission from Ref. [132]. Copyright 2015, American Chemical Society. **d** High-resolution of O 1*s* XPS core level spectra of ZnO with annealing at 200 °C for 1 h in air. **e** XRD patterns and photographs of perovskite film on annealed ZnO without thermal annealing and annealing at 100 °C for 30 min. **d, e** Reproduced with permission from Ref. [133]. Copyright 2015, American Chemical Society. (Color figure online)

reduced electron mobility of ZnO and deteriorative chemical stability of PSCs. This neutralization reaction can be presented in the following reaction [127]:

$$2HI + ZnO \rightarrow ZnI_2 + H_2O \qquad (49)$$

SnO$_2$ is widely used in PSCs owing to its good electron transport ability and chemical stability. However, the interactions between the Cl-containing SnO$_2$ and perovskite still exist. Recently, Seok et al. reported that a FASnCl$_x$ interlayer at a SnO$_2$/perovskite interface could be formed by an interfacial reaction between Cl-bonded SnO$_2$ and Cl-containing FAPbI$_3$ perovskite (Fig. 8a and b) [5], which is related to the easy formation of Sn-based perovskites in the presence of Cl$^-$, FA$^+$ and Sn^{2+} [133, 134]. The coherent interlayer reduces the interfacial charge recombination and enhances charge transport/extraction, achieving stable PSCs with a high PCE of 25.8% (Fig. 8c and d). However, Sn-Cl bonds

did not form when the Cl-containing FAPbI$_3$ solution was applied on a pure SnO$_2$ surface. In comparison, Cl-bonded SnO$_2$ can interact with Cl$^-$-free FAPbI$_3$ precursor to form Sn-I bonds by Cl$^-$–I$^-$ exchange. In addition, Pang et al. also discovered the spontaneous ion-exchange reaction between Cl$^-$ and I$^-$ at the SnO$_x$-Cl/MAPbI$_3$ interface (Fig. 8e and f), which could effectively passivate the physical contact defects. The diffusion of Cl$^-$ in the MAPbI$_3$ films promoted the grain longitudinal growth and decreased the GB density [135]. It is worth noting that the reactions between SnO$_x$–Cl and perovskite effectively passivate the interface defects, thereby improving the photovoltaic performance and chemical stability of the PSCs.

Fullerene derivatives, like phenyl-C$_{61}$-butyric acid methyl ester (PCBM) and [6, 6]-Phenyl-C71-butyric acid methyl ester (PC$_{71}$BM), are another type of popularly used electron transport materials particularly in inverted PSCs. It's
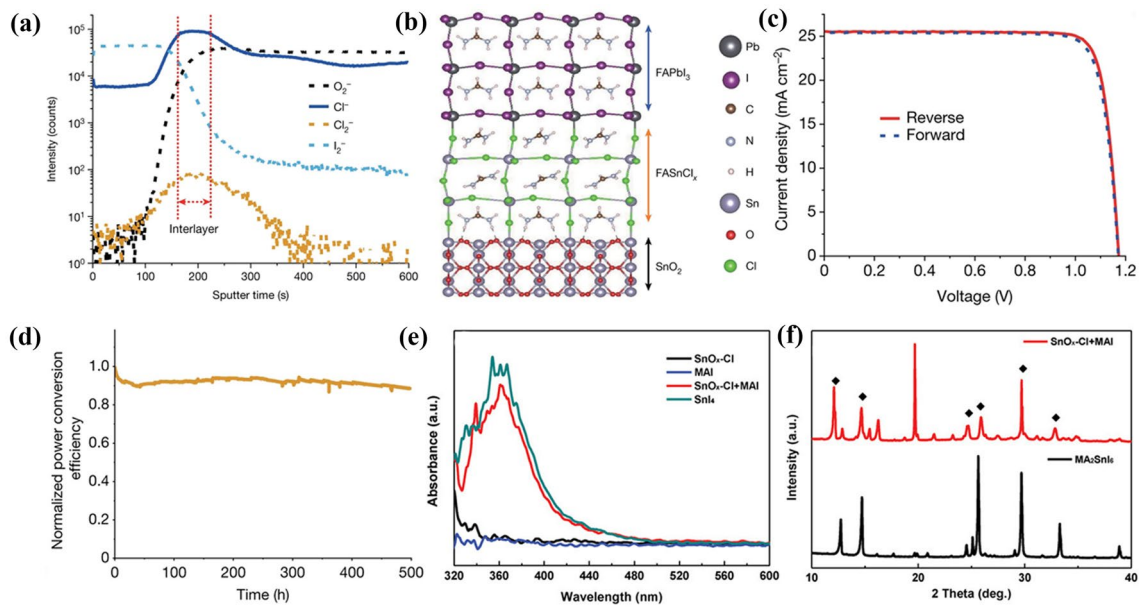
Fig. 8 **a** ToF-SIMS depth profiles for the perovskite and Cl-bonded SnO$_2$ on FTO. **b** Simulation of the formation of the FASnCl$_x$ interlayer between perovskite and SnO$_2$. **c** *J-V* curves of the best-performing device, measured in reverse (red solid line) and forward (blue dashed line) modes. **d** Maximum power point tracking measured for the PSC fabricated using Cl-bonded SnO$_2$ and Cl-containing FAPbI$_3$. **a-d** Reproduced with permission from Ref. [5]. Copyright 2021, Springer Nature. **e** UV-vis spectra of SnO$_x$-Cl, MAI, SnO$_x$-Cl+MAI, and SnI$_4$, respectively. **f** XRD pattern of SnO$_x$-Cl + MAI and reference MA$_2$SnI$_6$ powder samples, providing the feasibility of the ion-exchange reaction. **e, f** Reproduced with permission from Ref. [136]. Copyright 2019, Wiley-VCH. (Color figure online)

reported that PCBM undergoes an electron transfer reaction with halogens in perovskites to produce PCBM-nX radicals [74, 136]. Additionally, halogens favorably interact with C$_{70}$ face rather than O face of PC$_{71}$BM through covalent bonds [137]. Such strong interactions can suppress Pb-I antisite defects and ions migration at perovskite/PCBM interfaces, which can lead to improved stability and reduced hysteresis of PSCs [138]. However, C$_{60}$, another commonly used ETL in the inverted PSCs, barely undergoes interfacial chemical reactions with perovskites because of its chemical inertness.

2.2.2 HTL-Induced Reactions

In general, the widely used HTLs in inverted PSCs (i.e., p-i-n structure) are mainly poly(3,4-ethylenedioxythiophene) polystyrene sulfonate (PEDOT:PSS) [139, 140], poly[bis(4-phenyl)(2,4,6-trimethylphenyl)amine] (PTAA) [141–143] and NiO$_x$ [144, 145]. As an inorganic HTL, NiO$_x$ is regarded as a promising HTL candidate with the advantages of good optical transparency, excellent stability

and low cost [146, 147]. The interaction between NiO$_x$ and perovskite has been studied by many groups. McGehee et al. proposed a surface-assisted electron transfer-proton transfer (ET-PT) reaction mechanism at the NiO$_x$/perovskite interface [148]. They deposited various perovskite precursors (MAI, MABr, MACl, CsI, and PbI$_2$ in acetonitrile solvent, respectively) onto NiO$_x$ surface and observed that only MAI could bleach NiO$_x$ film, which demonstrates that Ni$^{\geq 3+}$ sites can oxidize I$^-$ only in the presence of a proton donor but neither Br$^-$ or Cl$^-$ because of their much higher oxidation potentials. In conclusion, Ni$^{\geq 3+}$ defect sites can act not only as Lewis acid to oxidize I$^-$ but also as Brønsted base to deprotonate CH$_3$NH$_3^+$. The perovskite solution was deposited on the various HTLs (PTAA, poly-TPD, and NiO$_x$) to detect the differences in the perovskite films through XRD analysis. It's observed that PbI$_2$ accumulates at the NiO$_x$/perovskite interface or scatters throughout PTAA-based perovskite. However, only the interfacial PbI$_2$ can block the extraction of holes resulting in the V_{oc} loss of PSCs. The whole reaction can be shown in Fig. 9a.
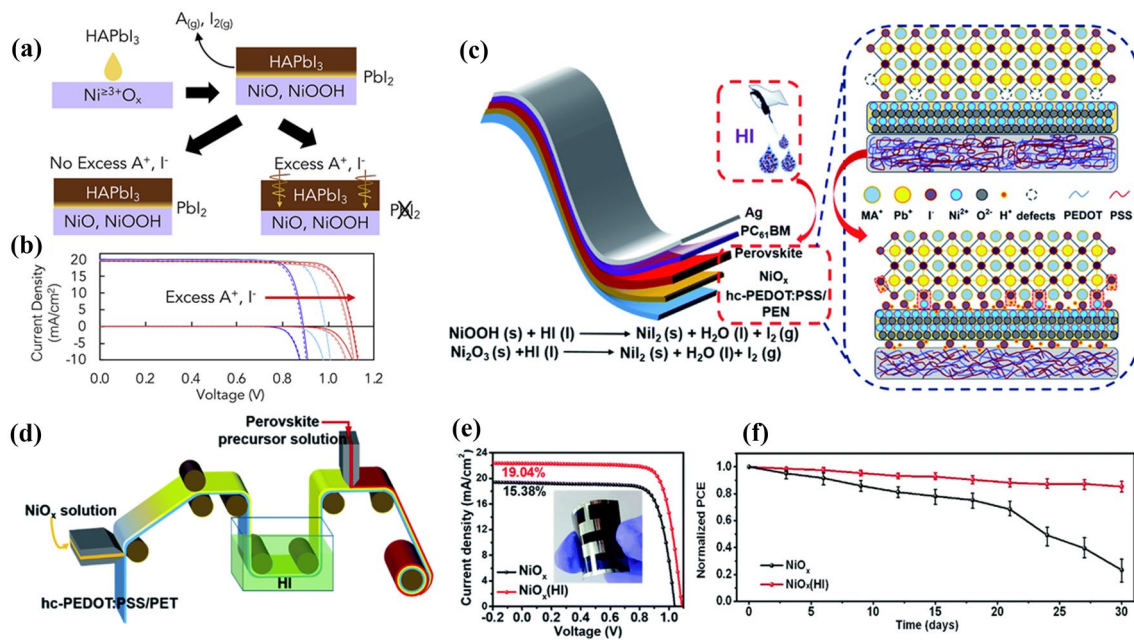
Fig. 9 **a** Schematic of the formation process of $PbI_{2-x}Br_x$ at the interface. **b** Dark and light *J-V* curves of $Cs_{0.25}FA_{0.75}Pb(Br_{0.2}I_{0.8})_3$ perovskite solar cells with 0–3 mol% excess A-site. **a**, **b** Reproduced with permission from Ref.[150]. Copyright 2020, Elsevier. **c** Diagram of the passivation mechanism. **d** Fabrication procedure for perovskite solar cells by R2R process. **e** *J-V* curves of flexible devices (1.01 cm^2) with and without HI treatment. Inset presents the photograph of flexible perovskite solar cells. **f** Normalized PCE of encapsulated PSCs based on NiO_x and NiO_x (HI) hole-transport layers under ambient condition (25–55% relative humidity and 25–35 ℃) for 30 days. **c-f** Reproduced with permission from Ref. [146]. Copyright 2021, Royal Society of Chemistry

$$(CH_3NH_3)PbI_3 + Ni^{\geq 3+}O_x \leftrightarrow Ni^{\geq 2+}O_xH + PbI_2 + CH_3NH_2 \uparrow + \frac{1}{2}I_2$$
(2.2-10)
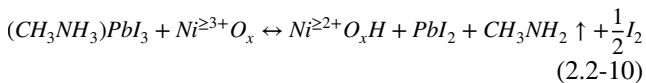
According to reaction Eq. 2.2-10, the resulting A-site deficient in this region increases interface recombination and reduces chemical stability of PSCs. The study found that 1–5 mol% excess A-site cations were incorporated into the perovskite precursor solution to prevent the reaction above. Therefore, the formation of PbI_2 layer at the NiO_x/perovskite interface is inhabited, and the V_{oc} was improved by > 200 mV as shown in Fig. 9b.

Wang et al. reported that trivalent nickel compound (NiOOH) on NiO_x HTL surfaces can be reduced to nickel iodide (NiI_2) by soaking the NiO_x HTLs in hydroiodic acid (HI) during roll-to-roll printing of flexible PSCs [144], as shown in Fig. 9c and d, which can enhance NiO_x/perovskite interface contact and ameliorate the work function of NiO_x film. The reaction process is shown below:

$$NiOOH + 3HI \rightarrow NiI_2 + 2H_2O + \frac{1}{2}I_2$$
(2.2-11)

$$Ni_2O_3 + 6HI \rightarrow 2NiI_2 + 3H_2O + I_2$$
(2.2-12)
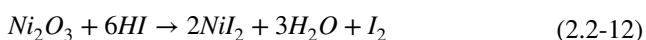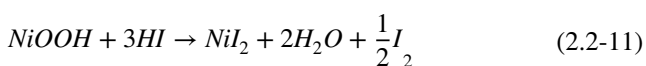
Subsequently, I^- in NiI_2 can coordinate with Pb in perovskite to form a Pb-I bond, inducing an orderly growth of perovskite lattice and enhancing the crystallinity of the perovskite film. Consequently, flexible PSCs with improved PCE as well as remarkable chemical stability were achieved (Fig. 9e and f).

In addition to NiO_x, the commonly used HTLs are PEDOT:PSS and PTAA in inverted PSCs. We note that PEDOT:PSS and PTAA are rarely reported to react with perovskites. However, PEDOT:PSS has been shown to corrode ITO due to its acidic composition, which can react with In_2O_3 [13, 139, 149, 150]. As a consequence, the dissociated indium ions can diffuse into the perovskite layer and then deteriorate device performance and stability [151, 152].

The normal PSCs (i.e. n-i-p structure) using 2,2',7,7'-Tetrakis[N,N-di(4-methoxyphenyl)amino]-9,9'-spirobifluorene (spiro-OMeTAD) as HTL have achieved efficiency records, however, the instability of spiro-OMeTAD itself and its additives limits their commercial applications [153]. Therefore, the interfacial reactions between perovskite and spiro-OMeTAD under various conditions have been investigated to improve the device

stability. Sultana et al. detected the signal of [spiro-OMeTAD(PbI$_2$)$_n$PbI]$^+$ adducts in the mass spectra and found that the interaction between spiro-OMeTAD and perovskite was beneficial for PSCs operations [38]. In addition, Belmonte et al. reported that I$^-$ is driven towards the spiro-OMeTAD HTL and react with the oxidized spiro-OMeTAD$^+$ under a positive bias (Eq. 2.2-13) [49]. This irreversible reaction turns the spiro-OMeTAD$^+$ into neutral molecule, which prevents the oxidation of spiro-OMeTAD [154] and consequently decreases the conductivity of HTL. Hence, this process has a negative effect on the photovoltaic performance and chemical stability of PSCs.

$$spiro - OMeTAD^+ + I^- \rightarrow spiro - OMeTAD - I \quad (2.2\text{-}13)$$
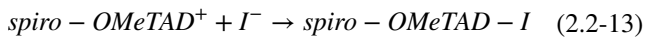
Besides, several common additives such as Lithium bis(trifluoromethanesulfonyl)-imide (Li-TFSI) and 4-tert-butylpyridine (TBP) in spiro-OMeTAD can influence the stability of perovskite active layers. Many studies have shown that the hygroscopic nature of Li-TFSI can accelerate the degradation of perovskite in humid conditions [155, 156]. As shown in Fig. 10a and b, TBP can react with PbI$_2$ to form new complexes [PbI$_2$ • xTBP], which disintegrates the perovskite structure and deteriorates the device performance [157, 158]. The reaction can be expressed as follows:

$$PbI_2 + xTBP \rightarrow PbI_2 \cdot xTBP \quad (2.2\text{-}14)$$

Chen et al. explored the decomposition of PSCs under operating conditions in the presence of light and H$_2$O [159]. The crystal evolution processes are displayed in Fig. 10c. As
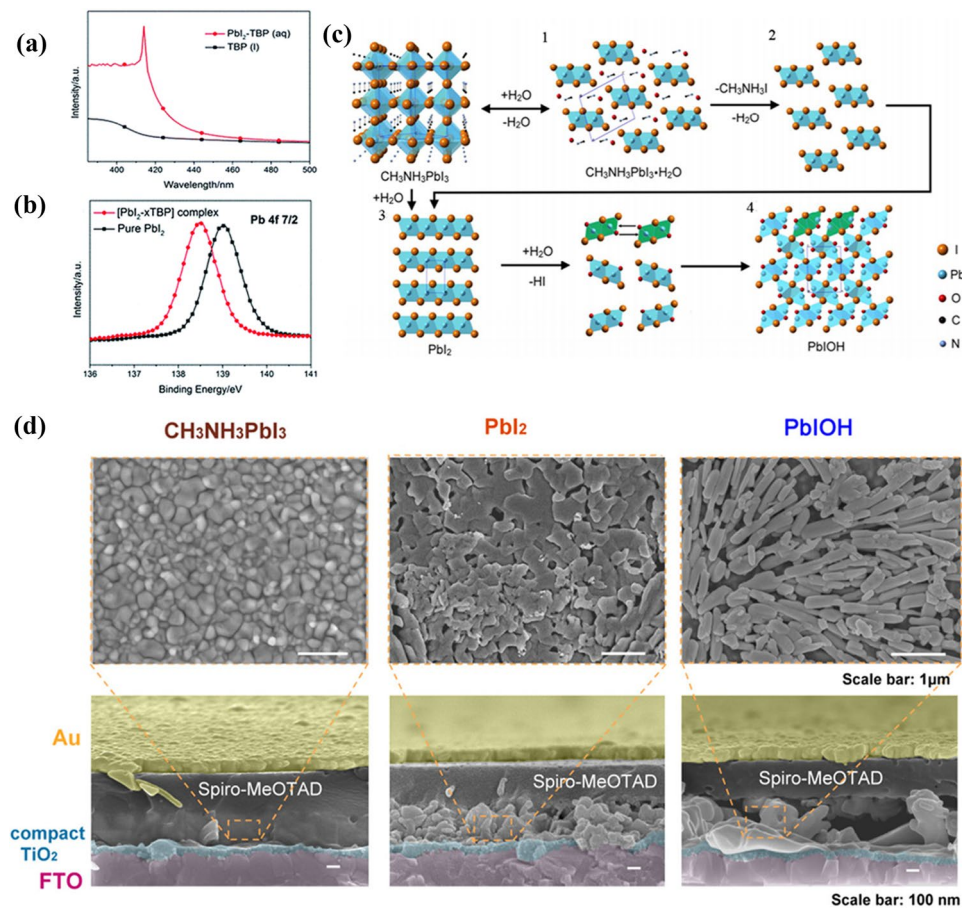

Fig. 10 **a** The UV-vis absorption of TBP liquid (dark line) and PbI$_2$ solution in TBP (red line). **b** Pb 4f7/2 XPS spectra consuming of PbI$_2$. **a**, **b** Reproduced with permission from Ref. [159]. Copyright 2014, Royal Society of Chemistry. **c** Crystal structural evolution from CH$_3$NH$_3$PbI$_3$, CH$_3$NH$_3$PbI$_3$·H$_2$O and PbI$_2$ to PbIOH. **d** FE-SEM images of top views and the cross-section views of relevant phases CH$_3$NH$_3$PbI$_3$, PbI$_2$, and PbIOH formed in lead halide perovskite solar cell at different stages. **c**, **d** Reproduced with permission from Ref. [161]. Copyright 2017, American Chemical Society

mentioned in Sect. 2.1.1, MAPbI$_3$ can react with H$_2$O generating intermediate CH$_3$NH$_3$PbI$_3$·H$_2$O in low-humidity conditions [63, 95, 96], which has little effect on the device performance. However, CH$_3$NH$_3$PbI$_3$·H$_2$O can further decompose into PbI$_2$ once exposed to high humidity, destroying the perovskite structure and reducing the chemical stability of PSCs. H$_2$O would further react with axial I of [PbI$_6$]$^{4-}$ to form [PbI$_4$O$_2$]$^{6-}$ under light irradiation or in the presence of spiro-MeOTAD. Given that the ionic radius of I$^-$ (2.06 Å) is significantly bigger than that of O^{2-} (1.26 Å) [136], [PbI$_4$O$_2$]$^{6-}$ is prone to deform. These deformed [PbI$_4$O$_2$]$^{6-}$ octahedrons further connect with each other to become PbIOH with the coordination structure of [PbI$_5$O$_3$]$^{9-}$. Figure 10d presents the scanning electron microscopy (SEM) images of PSCs at different degradation stages. It's worth noting that in addition to H$_2$O and light, spiro-MeOTAD is another key factor to stimulate the decomposition of MAPbI$_3$ into PbIOH, indicating that spiro-OMeTAD has a crucial influence on the chemical stability of PSCs.

Because of the intrinsic thermal instability of organic HTLs in normal PSCs, a lot of research efforts are devoted to inorganic HTLs [160–162], such as CuSCN, which is a promising candidate due to its low cost and durability [163–165]. It's reported that the CuSCN can catalyze the thermal degradation process of perovskite films even in the absence of moisture and oxygen [82, 166–168], although the thermal stability of CuSCN itself is excellent. CH$_3$NH$_3$I and CuSCN can react to form CH$_3$NH$_3$SCN and CuI as follows:

$$(CH_3NH_3)PbI_3 + CuSCN \xrightarrow{heat}$$
$$CuI + PbI_2 + CH_3NH_3SCN \qquad (2.2\text{-}15)$$
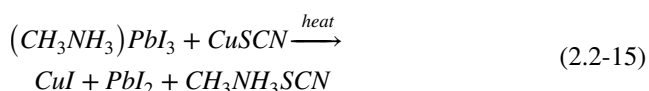
2.3 Metal Electrodes

Lead halide perovskites not only react with the adjacent layers like charges transport layers, but also experience chemical interactions with the top metal electrodes through ions migrations. The common metal electrodes, such as aluminum (Al), silver (Ag) and gold (Au), can be corroded when in contact with hybrid perovskites or air. These metal ions can diffuse through charge transport layers into perovskites and meanwhile the halide species like I$^-$ can migrate to the metal electrode, which result in reactions between metal and halide ions. It has been reported that almost all reactions between metal electrode and perovskites cause severe performance

and stability deterioration of PSCs. Therefore, exploring the reactions of the metal electrodes is helpful to have a better understanding of the chemical stability issues of PSCs.

2.3.1 Ag Electrode-Induced Reactions

Ag is prone to suffer from corrosion or contamination in contact with lead halide perovskite films. Studies found that I$^-$ in perovskites can react with spiro-OMeTAD$^+$ at the interface, resulting in a large amount of I$^-$ accumulating in the spiro-OMeTAD layer [49, 169]. Strikingly, I$^-$ passes through the Spiro-OMeTAD layer and migrates to the Ag contact, meanwhile, Ag ions also diffuse into the perovskite layer from the top electrode, generating AgI in the PSCs [93, 170, 171].

Kato et al. reported that moisture can promote the production of AgI and a five-steps mechanism is proposed to understand the observations (Fig. 11a) [171], including (1) diffusion of H$_2$O into perovskite through the pinholes in spiro-MeOTAD layer; (2) H$_2$O-induced decomposition of MAPbI$_3$ and production of volatile species containing I$^-$ (e.g., HI); (3) Migration of these volatile species to the bottom or top Ag layer; (4) Surface diffusion of the volatile species containing I$^-$; (5) AgI formation. The chemical reaction of AgI formation can be expressed as follows:

$$2HI + 2Ag \rightarrow 2AgI + H_2 \uparrow \qquad (2.3\text{-}1)$$

In addition, thermal treatment can also accelerate the formation of AgI in inverted PSCs. In Fig. 11b–d, time-of-flight secondary ions mass spectroscopy (ToF–SIMS) tests revealed that thermal treatment triggered a significant accumulation of I$^-$, I$_2^-$, and CN$^-$ ions at the PCBM/Ag interface, indicating two crucial facts: the decomposition of MAPbI$_3$ and the diffusion of both I$^-$ and MA$^+$ ions [172]. The formation of AgI accelerates the release of MA$^+$ and I$^-$ ions from the GBs of the perovskite layer and reconstructs the grain domains, leading to more defects both in the perovskite films and at the interface. Consequently, the PSCs suffer from degraded performance due to the formation of AgI.

Ma et al. reported electrochemical corrosion of Ag grid electrodes by PEDOT:PSS in flexible PSCs, which is a major reason for the low performance and poor chemical stability of the devices [41]. This redox reaction involves the reduction of the highly conductive PEDOT:PSS layer and the oxidation of the Ag electrode, which is proposed
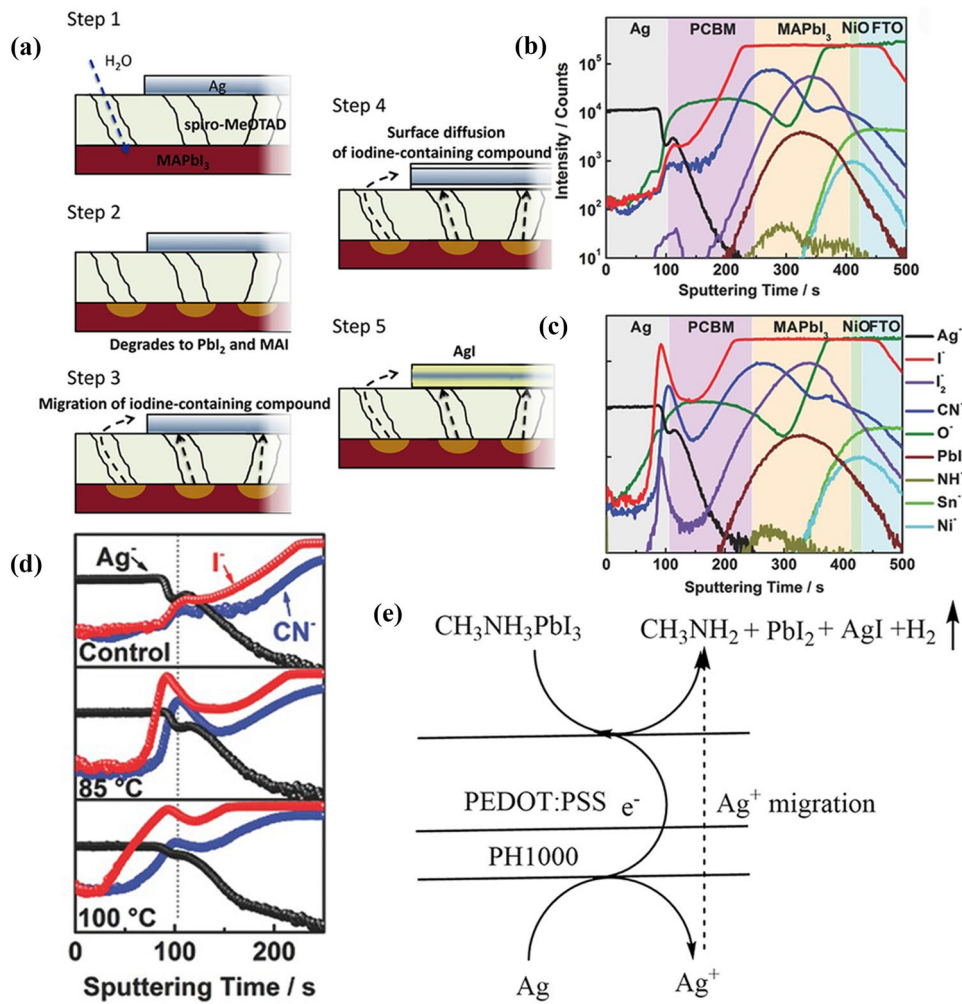
Fig. 11 **a** Schematic illustration of a proposed mechanism of AgI formation. Reproduced with permission from Ref. [174]. Copyright 2015, Wiley-VCH. ToF-SIMS elemental depth profiles **b** before and **c** after a thermal treatment at 85 °C for 24 h. **d** The depth profiles of Ag⁻, I⁻ and CN⁻ after different temperature of thermal treatment. **b-d** Reproduced with permission from Ref. [175]. Copyright 2017, Wiley-VCH. **e** The possible reaction mechanism of the PH1000-involved electrochemical corrosion of Ag electrode. Reproduced with permission from Ref. [41]. Copyright 2018, Wiley-VCH

to be three steps including (Fig. 11e): (1) Ag electrode easily loses an electron to form Ag⁺ with the aid of acidic PEDOT:PSS layer; (2) PEDOT:PSS layer receives an electron and is reduced; (3) Ag⁺ enters into the perovskite precursor solution and reacts with I⁻ to generate AgI.

Therefore, regardless of the structure of PSCs, the corrosion of Ag electrode is usually ascribed to the chemical reactions between Ag and the components of perovskites, which is achieved through Ag⁺ migration or halide ions diffusion [173–175]. Eventually the formed AgI impedes the charge transport and reduces the photovoltaic performance and chemical stability of PSCs.
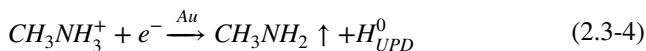
2.3.2 Au Electrode-Induced Reactions

Au, an inert metal and a common electrode material [5, 176], has been found to react with lead hybrid perovskite in previous studies [177–181]. Researches show that Au diffuses from the electrode across the HTL into the perovskite layer under certain conditions such as light soaking [182] or heat aging [183], resulting in an irreversible loss in photovoltaic performance and chemical stability of PSCs. Tarasov et al. proposed the corrosion mechanism of Au electrode based on its reaction with iodine-based perovskites [184]. Generally, the intensive UV irradiation of perovskite would induce the

release of volatile I_2 and MAI, forming highly reactive polyiodide melts with a general formula of MAI-nI_2. This MAI-nI_2 could react strongly with Au at room temperature and form $[AuI_2]^-$ and $[AuI_4]^-$ complexes. Consequently, a new $(MA)_2Au_2I_6$ phase is observed on the Au interface, which is detrimental to the performance of PSCs.

$$2MAI - nI_2 + 2Au \xrightarrow{light} (MA)_2Au_2I_6 \qquad (2.3-2)$$
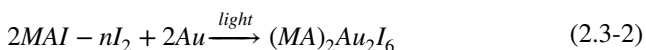
In addition, MAPbI₃/Au interface can catalyze the perovskite degradation reaction. A type of reduction/oxidation reaction termed underpotential deposition (UPD) involving lead, iodine, and hydrogen can occur at the MAPbI₃/Au interface [185]. UPD is a surface adsorption reaction that changes the oxidation state of ions, and occurs spontaneously at a lower voltage than the bulk reaction potential. XPS measurements demonstrate that Pb^0_{UPD} and I^0_{UPD} form at MAPbI₃/Au surface, and the whole degradation pathway of MAPbI₃/Au can be described with the following steps (Fig. 12a): (1) I^- loses an electron to form I^0_{UPD} that absorbs on the Au surface (Eq. 2.3-3), which induces the decomposition of MAPbI₃ into PbI₂ and $CH_3NH_3^+$. (2) $CH_3NH_3^+$ captures a free electron to form methylamine gas and H^0_{UPD} simultaneously (Eq. 2.3-4). (3) The adsorbed I^0_{UPD} reacts with H^0_{UPD} to generate HI, I_2, or H_2 gases (Eq. 2.3-5, 2.3-6, 2.2-7). (4) The byproduct CH_3NH_2 reacts with PbI₂ via PbI (CH_3NH_2) interphase to form more

HI, imines, and Pb^0_{UPD} (Eq. 2.3-8). Eventually, the degradation reaction of MAPbI₃ will stop when the surface of the Au catalyst is completely covered with Pb^0_{UPD}. Hence, the detrimental interfacial chemical reactions provide a source for defects and reduce the chemical stability of PSCs.

$$I^- \xrightarrow{Au} I^0_{UPD} + e^- \qquad (2.3-3)$$

$$CH_3NH_3^+ + e^- \xrightarrow{Au} CH_3NH_2 \uparrow + H^0_{UPD} \qquad (2.3-4)$$

$$I^0_{UPD} + H^0_{UPD} \rightarrow HI \uparrow \qquad (2.3-5)$$

$$2I^0_{UPD} \rightarrow I_2 \qquad (2.3-6)$$

$$2H^0_{UPD} \rightarrow H_2 \uparrow \qquad (2.3-7)$$

$$CH_3NH_2 + PbI_2 \xrightarrow{Au} CH_2 = NH \uparrow + Pb^0_{UPD} + 2HI \uparrow \qquad (2.3-8)$$

Notably, Au not only reacts with perovskite through ions migrations but also can be corroded by interaction with the inorganic holes transport material CuSCN. It has been reported that the reactive thiocyanate anions are prone to react with Au electrode under an electrical bias, forming an undesired potential barrier for charge carriers [153, 165,
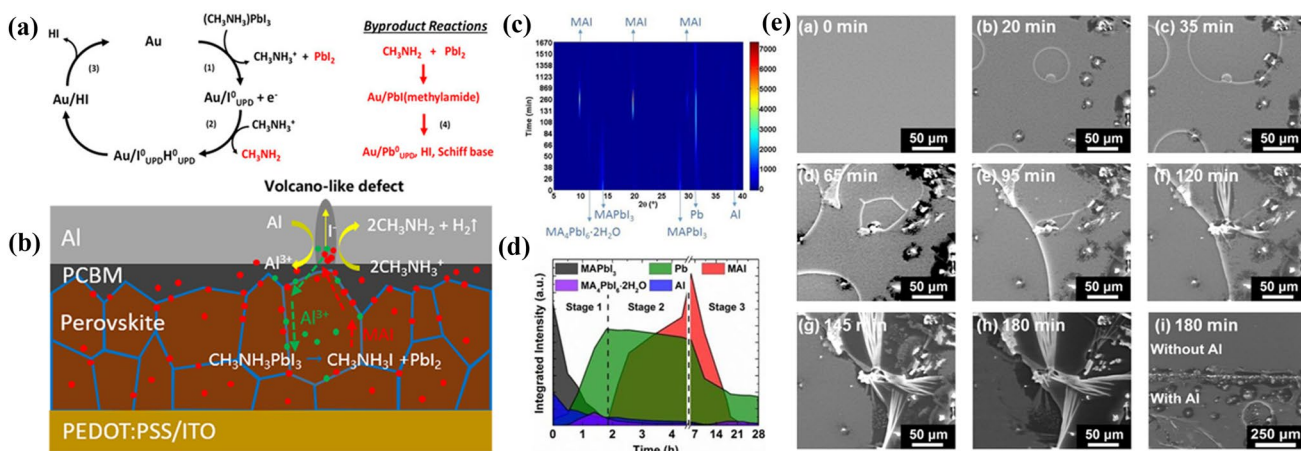

Fig. 12 **a** Proposed noble metal catalyzed degradation at MAPbI₃/Au heterojunctions where the byproducts methylamine and PbI₂ (in red) lead to the eventual formation of Pb⁰. Reproduced with permission from Ref. [188]. Copyright 2019, American Institute of Physics. **b** Proposed chemical corrosion of Al electrode of p-i-n type PSCs by the diffusion of CH₃NH₃I. Reproduced with permission from Ref. [192]. Copyright 2020, Wiley-VCH. In situ XRD analysis of the degradation of the LED stack with moist air in the dark: **c** In situ XRD spectra versus time. **d** Integrated XRD peak intensities of key materials versus time. **e** In situ SEM analysis on the LED stack in an environmental chamber at various time points from 0 to 180 min; the last one, SEM image near the boundary of the Al area after 180 min exposure showing that only the area covered with Al undergoes H₂O-mediated decomposition. **c**–**e** Reproduced with permission from Ref. [193]. Copyright 2016, American Chemical Society

186, 187], which may seriously affect the device performance and chemical stability.
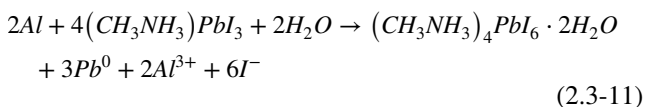
2.3.3 Al Electrode-Induced Reactions

Although Al is commonly employed as the top electrode in inverted PSCs, Al is chemically unstable due to its easy oxidation by air and reactions with lead halide perovskites [171, 188]. For example, Ma et al. found that both $CH_3NH_3^+$ and I^- can migrate towards the Al electrode through a $PC_{61}BM$ layer, resulting in the chemical corrosion of the Al electrode and the degradation of the perovskite film [189]. In particular, CH_3NH_3I is highly acidic and can react with Al as shown below:

$$6CH_3NH_3I + 2Al \rightarrow 6CH_3NH_2 \uparrow + 2AlI_3 + 3H_2 \uparrow \quad (2.3\text{-}9)$$
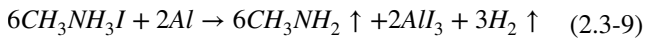
For the overall degradation of PSC, the chemical corrosion of Al electrode can be described in Eq. 2.3-10. The reaction process involves the following steps (Fig. 12b) including: (1) formation of CH_3NH_3I from perovskite decomposition, (2) diffusion of CH_3NH_3I through the thin $PC_{61}BM$ region, (3) reaction between CH_3NH_3I and Al, yielding AlI_3, CH_3NH_2 and H_2, (4) formation of bubble and volcano-like surface defects owing to the release of H_2 gas, (5) further decomposition of perovskite due to the Al^{3+} diffusion into perovskite layer.

$$6(CH_3NH_3)PbI_3 + 2Al \rightarrow 2AlI_3 + 6PbI_2 + 6CH_3NH_2 \uparrow + 3H_2 \uparrow$$
$$(2.3\text{-}10)$$
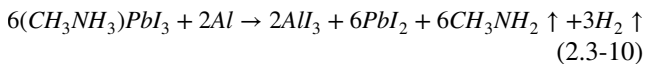
To further investigate the Al-perovskite reactions, Zhao et al. employed in situ X-ray diffraction (XRD) analyses (Fig. 12c and d) and SEM measurements (Fig. 12e) to study the redox reactions between the Al electrode and perovskite [190]. The chemical degradation process can be divided into three stages. Stage 1: Al reacts with a perovskite in the presence of moisture, resulting in the reduction of Pb^{2+} to Pb^0 and the crystal nucleation of $MA_4PbI_6 \cdot 2H_2O$, which can be expressed as follows:

$$2Al + 4(CH_3NH_3)PbI_3 + 2H_2O \rightarrow (CH_3NH_3)_4PbI_6 \cdot 2H_2O$$
$$+ 3Pb^0 + 2Al^{3+} + 6I^-$$
$$(2.3\text{-}11)$$

Stage 2: with the continuous redox reaction between Al and Pb^{2+}, the further loss of Pb^{2+} in $MA_4PbI_6 \cdot 2H_2O$ will lead to the formation of MAI as shown below:

$$2Al + 3(CH_3NH_3)_4PbI_6 \cdot 2H_2O \rightarrow 12CH_3NH_3I$$
$$+ 3Pb^0 + 2Al^{3+} + 6I^- + 2H_2O$$
$$(2.3\text{-}12)$$
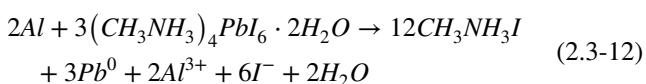
Stage 3: Once metal Al is completely oxidized to Al^{3+}, further exposure to moisture could cause Pb^0 to reoxidize and hydrate forming $PbO \cdot xH_2O$. In addition, volatile MAI gradually disappears due to prolonged exposure to air. Here, moisture not only promotes ions diffusion but also keeps the reactions between Al and $MAPbI_3$ forward.

3 Strategies for Improving the Chemical Stability

Interfacial chemical reaction is a key factor affecting the chemical stability of lead halide PSCs. According to the above discussion, not all the interfacial reactions in PSCs are detrimental to device performance and chemical stability, such as the reactions at SnO_x-Cl/perovskite interface. Therefore, in order to improve the chemical stability of PSCs, it's necessary to inhibit unfavorable interfacial reactions. Two effective strategies have been proposed to reduce adverse interfacial reactions in the past few years. One is to insert a buffer layer at the contact interface to block ions migration or the invasion of water and oxygen. At present, many materials, such as PMMA [167], Al_2O_3 [82], and Cr_2O_3 [181], are introduced to optimize contact interfaces as a buffer layer. Another approach is to employ additives, such as 2-amylpyridine [158] and ionic liquids [191], in perovskites to reduce the chemical activity of the reactants.

3.1 Buffer Layers

Various buffer layers have been developed to modify the perovskite surface to prohibit the chemical reactions with various materials, including air, NiO_x, spiro-OMeTAD, CuSCN, TiO_2, ZnO, metal electrode and so on, based on different reaction mechanisms. The effective approaches for these interface modifications are detailed as follows.

Air/perovskite interface: The buffer layer, especially polymer materials, can isolate moisture or oxygen and inhibit the degradation of lead halide perovskite films. For example, hygroscopic polymer poly(ethylene oxide) (PEO) can chemically interact with undercoordinated Pb ions on a perovskite surface, passivating defect sites and reducing charge recombination loss [192]. In Fig. 13a and b, PEO prevents surface hydration reaction of perovskite by absorbing H_2O before perovskites do, leading to greatly improved chemical stability of PSCs. A number of hydrophobic polymers, such

as polystyrene [193], PTzDPPBTz [91] and carbon-based materials [194], are also used to protect perovskites from H_2O. In Fig. 13c, Trichloro(3,3,3-trifl uoropropyl)silane was introduced between a perovskite layer and C_{60} ETL, which reacts with a tiny amount of H_2O existing in the perovskite film to form silanols [193]. Then these silanols can automatically cross-link through forming Si–O–Si (siloxane) bonds to make the insulating layer protect the underlying perovskite film from water erosion.

It has been reported that low-dimensional materials covering perovskite surfaces can effectively insulate O_2 and improve the perovskite film quality [58]. For example, Kanatzidis et al. inserted a 1D thiazole ammonium lead iodide ($TAPbI_3$) interfacial layer between the perovskite and HTL, which serves to passivate the three-dimensional (3D) perovskite film and prevent oxygen invasion [195], leading to an improvement of device efficiency as well as enhancement of chemical stability.

NiO_x/perovskite interface: The interfacial redox reaction between Ni^{3+} in NiO_x and MAI salt will generate PbI_2-rich holes extraction barriers, which can lower V_{oc} and accelerate perovskite degradation by deprotonating precursor amine and oxidizing iodide to interstitial iodine [148]. A modifier layer, trimethylolpropane tris(2-methyl-1-aziridinepropionate) (SaC-100), was used to modify the NiO_x/$MAPbI_3$ contact interface [83]. Results reveal that N and O atoms in SaC-100 can passivate the uncoordinated Ni^{3+} and Pb^{2+} defects in NiO_x and $MAPbI_3$ through
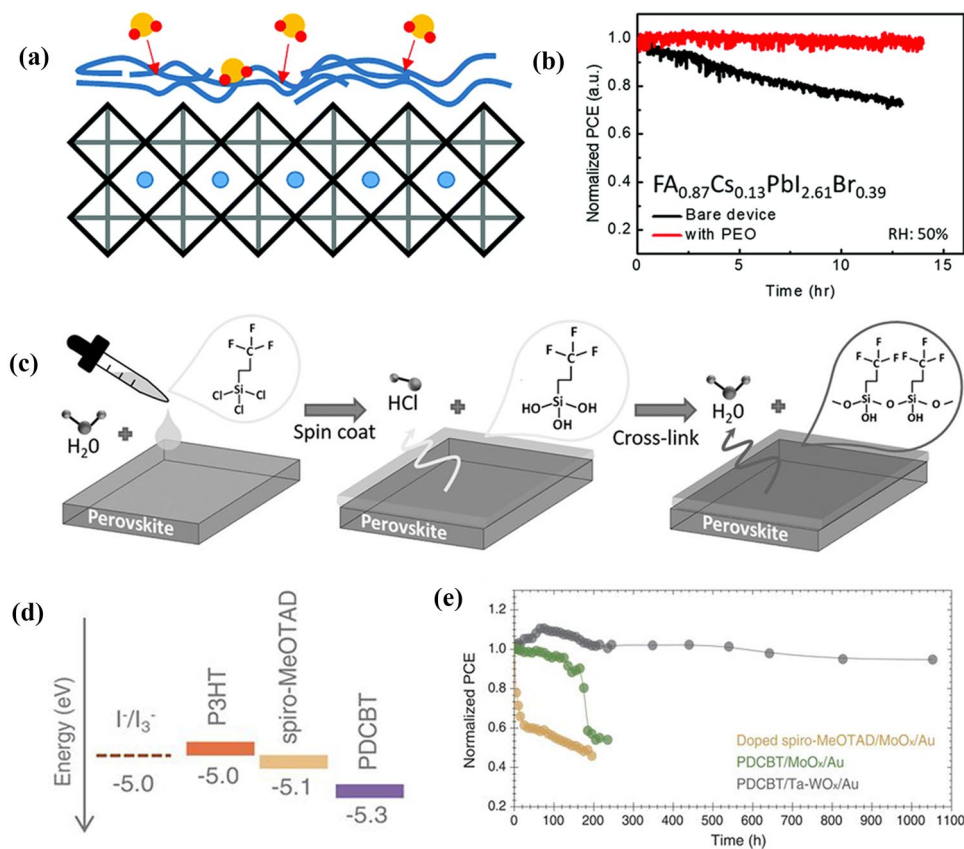

Fig. 13 **a** Schematic illustration of polymer PEO thin film assembled on the perovskite structure. **b** Operational stability test for evolution of PCE of $FA_{0.87}Cs_{0.13}Pb(I_{0.87}Br_{0.13})_3$ devices without and with PEO, continuously measured under xenon-lamp simulated fullspectrum AM 1.5, 100 mW cm^{-2} equivalent irradiance in air (humidity ~50 RH%) without any ultraviolet filter, held at maximum power point during ageing, and tested at 0.03-s time intervals. **a, b** Reproduced with permission from Ref. [195]. Copyright 2018, Royal Society of Chemistry. **c** Schematic diagram showing the cross-link process of fluoro-silane layer on the perovskite film. Reproduced with permission from Ref. [196]. Copyright 2016, Wiley-VCH. **d** The corresponding redox potential of I^-/I_3^- and the homo levels of P3HT, PDCBT, and spiro-MeOTAD. **e** The unencapsulated device photostability tests under continuous one sun illumination in a home-built chamber filled with N_2. **d, e** Reproduced with permission from Ref. [199]. Copyright 2017, AAAS

producing Lewis adducts, respectively. In addition, the reaction between NiO_x and $MAPbI_3$ is suppressed in the presence of SaC-100, which is helpful for improving the conductivity of NiO_x and inhibiting the degradation of $MAPbI_3$ films.

Spiro-OMeTAD/perovskite interface: Buffer layer materials can not only resist the invasion of air, but also block the undesired contacts between adjacent layers. For example, Wang et al. reported an effective buffer layer montmorillonite (MMT), which was inserted between perovskite and spiro-OMeTAD to prevent TBP from reacting with PbI_2, because MMT can interact with TBP and build its intercalated structure by hydrogen bond. Consequently, the efficiency and chemical stability of PSCs are largely improved simultaneously [157]. I_2 deriving from perovskite tends to react with HTLs, such as Spiro-OMeTAD, whose HOMO level is close to the oxidation potential of I^-/I_3^- (~ -5.0 eV). In Fig. 13d, depositing a polythiophene derivative with a lower HOMO level approaching -5.3 eV on the perovskite surface can effectively suppress I^-/I_3^- reaction, resulting in PSCs with enhanced efficiency and stability (Fig. 13e) [196].

CuSCN/perovskite interface: In order to promote the chemical stability of PSCs with CuSCN HTLs, it's necessary to insert a buffer layer between perovskite and CuSCN. Snaith et al. not only introduced mesoporous Al_2O_3 at the perovskite/CuSCN interface to reduce the contact area of CuSCN with perovskite, but also encapsulated the complete cell with PMMA to prevent degradation products from release [82]. It has been found that if an electrical bias is applied on the PSC, an electrical potential-induced reaction between Au and SCN^- would occur, leading to poor operational stability of PSCs. Therefore, a thin reduced graphene oxide (rGO) interlayer was introduced between CuSCN and Au electrode to migrate the degradation reaction [165]. In addition, Cu_2O [197] and $Cs:NiO_x$ [198] interfacial layers were also used to reduce these detrimental interfacial chemical reaction for PSCs.

TiO$_2$/perovskite interface: Ito et al. performed light irradiation tests of PSCs with/without a Sb_2S_3 inserted layer between TiO_2 and $MAPbI_3$ [124]. For the device without Sb_2S_3, the black $MAPbI_3$ layers completely decompose to yellow PbI_2 by losing HI and CH_3NH_2. On the other hand, the device with Sb_2S_3 can deactivate the reaction of I^-/I_2 at the surface of TiO_2, so the $MAPbI_3$ layer is stable and durable against light exposure as shown in Fig. 14a.

ZnO/perovskite interface: A thin layer of MgO and protonated ethanolamine were in sequence deposited on the ZnO surface to resolve the poor chemical stability of ZnO-based device [199]. Moreover, 1,2-ethanedithiol [200], poly(ethylenimine) [132] and graphene oxide quantum dots [126] can also play the same role.

Metal/perovskite interface: The chemical instability of PSCs induced by metal electrode corrosion can be suppressed by interfacial modifications. I^- in the perovskite can migrate to an Al electrode through PCBM layer to react with Al, forming aluminum iodide at the Al/perovskite interface. A bathocuproine (BCP) buffer layer has been reported to insert the interface between the Al
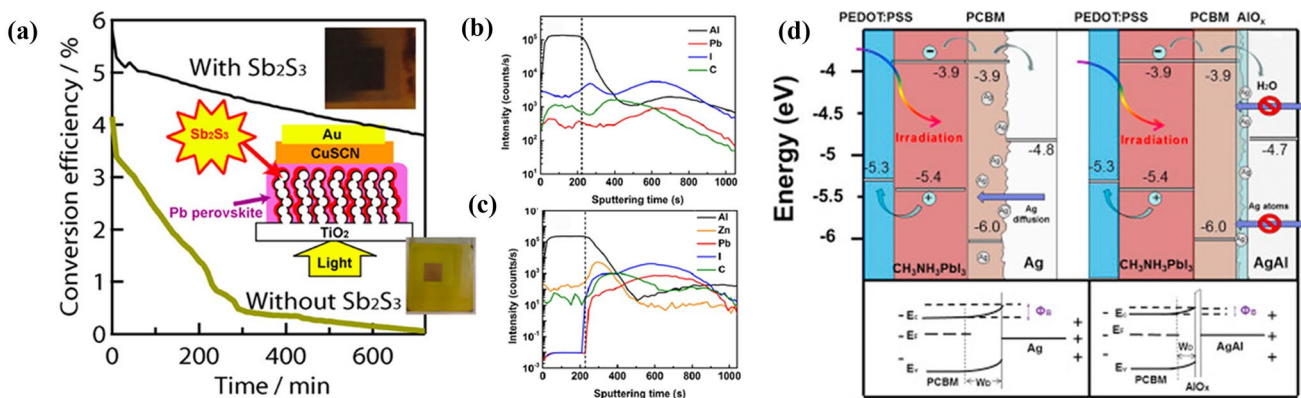

Fig. 14 **a** Variation of photoenergy conversion efficiencies of solar cells during light exposure (AM1.5, 100 mW cm^{-2}) without encapsulation in air for 12 h. Reproduced with permission from Ref. [125]. Copyright 2014, American Chemical Society. Composition depth profiles of the perovskite devices by SIMS: **b** with only PCBM as ETL; **c** with PCBM/ZnO bilayer as ETL. **b, c** Reproduced with permission from Ref. [204]. Copyright 2015, Elsevier. **d** Schematic energy level diagrams of cells with PCBM/Ag and PCBM/AgAl. Reproduced with permission from Ref. [206]. Copyright 2016, Elsevier. (Color figure online)

electrode and PC$_{61}$BM [189]. Test results support that this buffer layer can block the CH$_3$NH$_3$I migration and hence prevent the Al electrode from chemical corrosion by CH$_3$NH$_3$I, improving the chemical stability of the PSCs. Qiu et al. introduced a ZnO layer between PCBM and an Al electrode to prevent perovskite from reacting with Al, ToF–SIMS characterizations demonstrated that ZnO layer can effectively inhibit the diffusion of I$^-$ ions (Fig. 14b and c) [201].

Cr/Cr$_2$O$_3$ interlayer provides a buffer to shield top Ag electrodes from chemical corrosion caused by HI liberated from the MAPbI$_3$ degradation [181, 202]. Compared with pure Ag, an AgAl alloy electrode shows much higher stability in aging tests, which is related to AlO$_x$ formed at the PCBM/AgAl interface during thermal evaporation and aging [203]. In Fig. 14d, this AlO$_x$ interlayer can suppress the migration of Ag atoms to the active layer, strengthen the metal contact with PCBM and prevent moisture encroachment. In addition, nanostructured carbon layers, including N-doped graphene, PCBM and carbon quantum dots, were inserted between a perovskite layer and an Ag electrode to block I$^-$ and Ag diffusion [204]. The degradation reaction of perovskite by ions migration was ultimately inhibited, and thus the chemical stability of PSCs was greatly enhanced. Moreover, a graphene barrier between CuSCN and Au can inhibit I$^-$ migration and perfectly block Au diffusion, as shown in Fig. 15a–c [205], successfully restraining undesired chemical reactions between I$^-$ and the Au electrode. Many groups introduced stable buffer layers through interfacial reactions to reduce ions migration [206]. For example, hexamethyldisilathiane is deposited on a perovskite surface to react with Pb^{2+} and form stable PbS buffer layer, which can effectively suppress I$^-$ diffusion and prevent corrosion of metal electrodes [207].

3.2 Additives Engineering

Water-induced reactions: Various additives have been demonstrated to change the physical or/and chemical properties of metal halide perovskites and thus improve the moisture-/oxygen-/light- stability of the materials [208]. For example, a fluorinated additive named 1,1,1-trifluoro-ethylammonium iodide (FEAI) was introduced into MAPbI$_3$ to reduce the moisture-induced degradation reactions, because the hydrophobic CF$_3$-terminal group on the perovskite surface resist the invasion of moisture [209]. Zhao et al. employed hygroscopic polyethylene glycol (PEG) scaffold to fabricate moisture-stable perovskite films because the omnipresent PEG molecules can absorb H$_2$O efficiently. The resulting compact moisture barrier around perovskite crystal grains can prevent water from penetrating into the films [210]. The additive ethyl 2-cyanoacrylate (E2CA) can spontaneously polymerize into a compact polymer once exposed to moisture as shown in Fig. 15d and e, blocking the penetration channels of moisture due to its hydrophobic nature [211]. Moreover, poly(4-vinylpyridine) (PVP) [212], poly(ethylene oxide) (PEO) [192], and trimethylolpropane triacrylate (TMTA) [213] can also be used as additives to reduce the reactions between perovskite and H$_2$O.

Oxygen-induced reactions: Snaith et al. introduced the ionic liquid 1-butyl-3-methylimidazolium tetrafluoroborate (BMIMBF4) into perovskite precursor and found that [BMIM]$^+$ cations were bound to the surface sites, hence suppressing the surface degradation reactions induced by oxygen or moisture adsorption (Fig. 15f) [214]. The thiourea has been demonstrated to form Pb–S bonds on the outermost layer of perovskite, which efficiently suppressed the absorption of oxygen and prevented the formation of superoxide [215].

Light-induced reactions: The solid ionic additive 1-butyl-1-methylpiperidinium tetrafluoroborate ([BMP]$^+$[BF$_4$]$^-$) was adopted to enhance the photostability of PSCs under full-spectrum sunlight [191]. It's reported that the generation of I$_2$ under illumination is one of the main factors causing the photo-degradation of perovskites [216]. The interstitial I$^-$ ions capture the holes to become neutral interstitial iodine atoms, and these neutral atoms need to diffuse and combine to produce I$_2$ [112]. [BMP]$^+$[BF$_4$]$^-$ therefore suppressed the photochemical reactions of perovskite by reducing the surface defects, such as interstitial pairs and iodide vacancies, and retarding diffusion of neutral iodine interstitials.

CTL-induced reactions: The additives can also inhibit undesirable reactions occurring at charges transport layer/perovskite interfaces. Han et al. used a new additive 2-amylpyridine (2-Py) to replace TBP in Spiro-OMeTAD and found that the corrosion of perovskite was suppressed [158]. The existence of the amyl chain at the ortho-position of pyridine in 2-Py is vital to restrain the perovskite degradation reaction, which is attributed to the following aspects: 1) the amyl chain near the nitrogen atom can reduce the
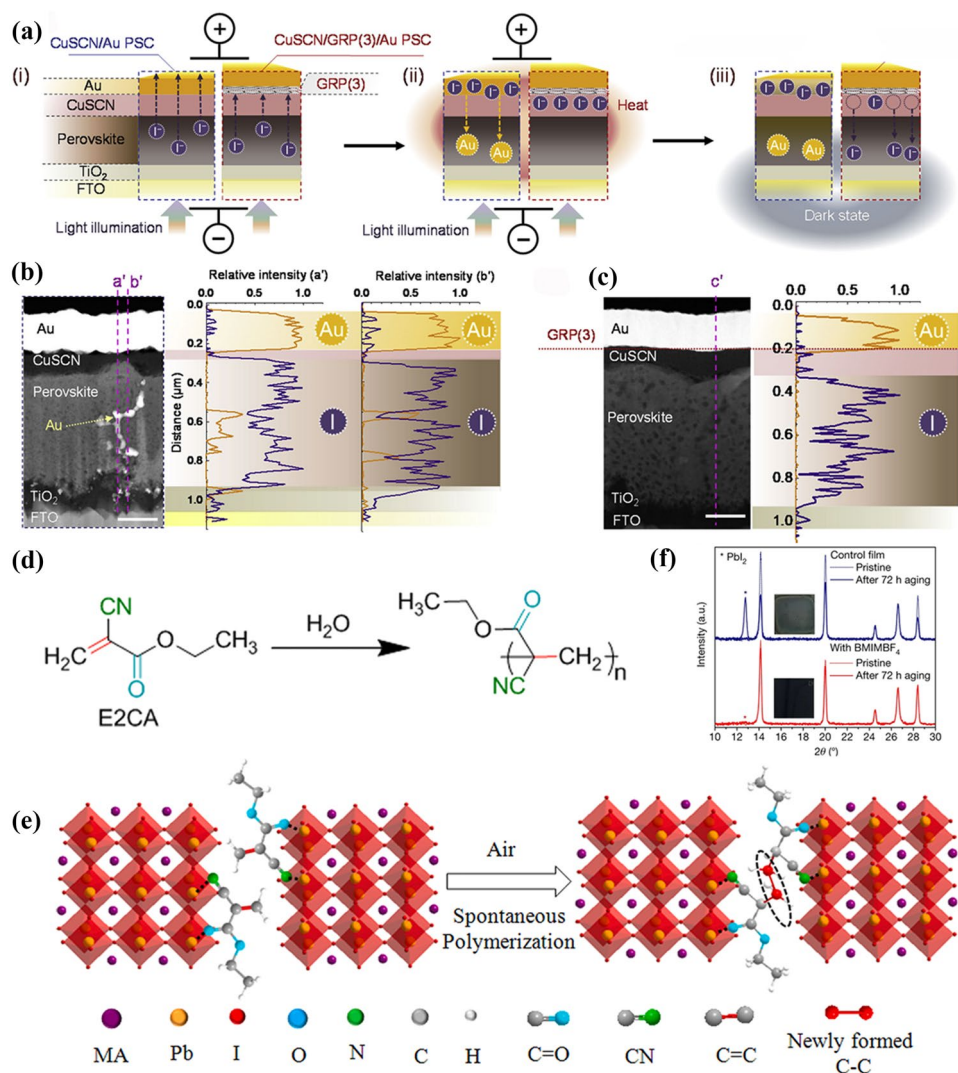
Fig. 15 The iodide ion (I⁻) and Au diffusion in CuSCN/Au and CuSCN/GRP (3)/Au PSCs. **a** Schematic of the diffusion process during the light illumination under an applied electrical bias and dark state without the bias. Cross-sectional STEM images of CuSCN/Au **b** and CuSCN/GRP (3)/Au PCSs **c** after 3 cycles of continuous light illumination (12 h) and dark state (12 h). The scale bar is 200 nm. The EDX scan (I and Au) along the vertical lines (a′, b′, and c′) are also provided. **a-c** Reproduced with permission from Ref. [208]. Copyright 2020, Elsevier. **d** Chemical structure and moisture induced polymerization of E2CA with marked functional groups: C=C (red), C≡N (olive) and C=O (cyan). **e** Schematic illustrations of spontaneous grain polymerization in MAPbI₃-E2CA films. E2CA chemically anchors to GBs with C=O and C≡N groups and spontaneously polymerizes to a polymer at GBs when exposed in moisture air. **d, e** Reproduced with permission from Ref. [214]. Copyright 2019, Elsevier. **f** XRD patterns of pristine and aged samples of control film and film containing BMIMBF₄ (0.3 mol%) on NiO/FTOcoated glass substrates. The stars represent the decomposition product of PbI₂ in the films. The insets show images of the aged samples (around 2.8 cm × 2.8 cm) after 72 h of light-soaking at 60-65 °C. Reproduced with permission from Ref. [217]. Copyright 2019, Springer Nature. (Color figure online)

coordination ability of pyridine; 2) the steric hindrance from the o-substitution of pyridine prevents it from penetrating the perovskite. In addition, 2-Py can increase the dissolution and dispersion of Li-TFSI compared with TBP, which has a positive effect on the conductivity of the Spiro-OMeTAD HTL. Other additives, like TiO_2 nanoparticles (NPs)-modified CNT (CNT:TiO_2) [217], graphene oxide (GO) [218],

and 1,6-diazidohexane (N3) [219] can also be introduced into spiro-OMeTAD to minimize the TBP-PbI₂ complex formation and hence improve the chemical stability of the perovskite/HTL interface.

Metal electrode-induced reactions: It has been reported that the ions migration can initiate the degradation of devices [113, 220], which can be efficiently inhibited by

some additives with special functional groups. For example, caffeine with two conjugated carboxyl groups interacts strongly with Pb^{2+} ions to slow down the perovskite crystal growth and thus produce high-quality films [221]. In Fig. 16, the Energy-dispersive X-ray spectra (EDX) mapping shows that Ag can diffuse into the whole perovskite region and I^- ions also migrate through the PTAA layer in the control device, while there is no obvious indication of such similar ions migrations in the caffeine-incorporated device. The caffeine significantly suppresses ions migration, and hence the chemical stability of PSCs is effectively enhanced. Chen et al. employed the methimazole (MMI) to form the MMI-PbI_2 complex in situ at the GBs, and these surface patches can also effectively suppress Ag diffusion and simultaneously retard I^- migration [222].

The multifunctional additive of dipentaerythritol pentaacrylate (DPPA) can impede I^- movements due to synergistic effects of its functional groups [223]. The $CH_2=CH$ groups in DPPA crosslink at GBs and block the channels of ions migrations. And the -OH groups in DPPA can bond with I^- in the perovskite through hydrogen bond interaction, chemically immobilizing these migrated I^-. In addition, the polystyrene (PS) [224] and PCBM [74] can also obstruct ions migrations across GBs and dissociated ions can only move around their original sites. Therefore, the problem of chemical stability induced by ions migration can be well solved.

4 Conclusions and Outlook

Although lead halide PSCs have already achieved a high certified PCE up to 25.7% through a low-cost and simple fabrication process, the long-term stability still lags far behind the commercial application standard. Therefore, the top priority is to explore the degradation mechanism of lead halide PSCs in more depth, which is helpful for achieving high-efficiency and stable devices. As one of the most important factors influencing the photovoltaic performance and chemical stability of PSCs, interfacial chemical reactions due to environment conditions, interface contacts and metal electrode are systematically elucidated in this paper. Their reaction mechanisms as well as influence on interface defects, non-radiative recombination and degradation process are summarized. Up to now, there is no unified theory that generalizes all interface reactions. For example, lead halide perovskites degrade easily to form PbI_2 and other lead-containing compounds once exposed to humid environment. O_2 capture photo-induced electrons to generate superoxide $O_2^{\cdot-}$ with the aid of light, which can induce quick degradation of lead halide perovskite films. In addition, some chemical reactions at charge transport layers/perovskite interface can produce undesirable interfacial defects and reduce charge transport capacity of ETL or HTL, eventually deteriorate the chemical stability and photovoltaic performance of PSCs. It's noteworthy that Cl-containing SnO_2 ETL can react friendly with lead halide perovskites to passivate the interface defects and improve the device efficiency. The interfacial reactions are
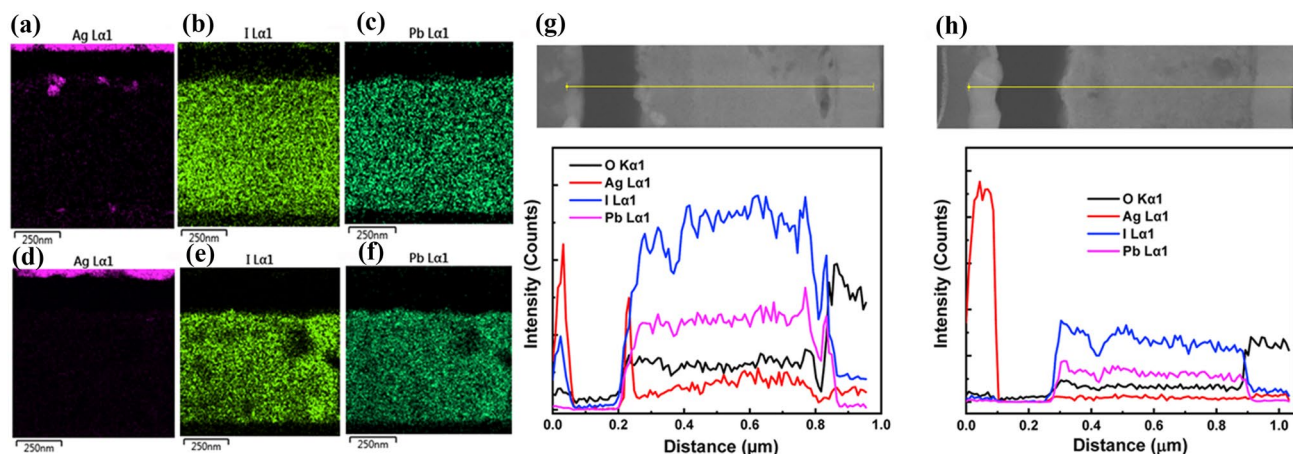

Fig. 16 **a-f** Energy-dispersive X-ray spectra (EDX) mapping of the aged pure PVSK device **a** Ag, **b** I, and **c** Pb, and the aged caffeine-containing PVSK device **d** Ag, **e** I, and **f** Pb. **g, h** EDX line scans of **g** aged pure PVSK device and **h** aged caffeine-containing PVSK device. Reproduced with permission from Ref. [224]. Copyright 2019, Elsevier. (Color figure online)

induced by ions migrations, for example, I⁻ can diffuse into a metal electrode and simultaneously metal ions can also migrate through the perovskite, which corrode the metal electrode and decrease the operational lifetime of PSCs.

At present, various buffer layers or additives have been employed to suppress the detrimental interfacial reactions and optimize the device performance as well as long-term stability. Therefore, it's necessary to investigate the chemical properties of additives or buffer layer materials in depth, because their different functional groups may play completely different roles in the photovoltaic performance. The fluorine-containing additives can improve the hydrophobic properties of lead halide perovskite films, and effectively reduce the humidity-induced degradation of PSCs. The detrimental I_2 in the lead halide perovskite easily induces the shallow charge traps and accelerates the light-decomposition of perovskite. The hydrazine functional group can reduce these I_2 in perovskite precursor solutions to I⁻, which significantly improve the light stability of perovskites. In addition, more attentions should be paid to benign chemical reaction in PSCs and thus we can make use of these reactions to further improve the efficiency and stability of PSCs. For example, the organic long chain amine (e.g. phenylethylamine, butylamine) can react with PbI_2 to form stable 2D perovskite on the bulk perovskite surface, contributing to the decreased non-radiative recombination and enhanced water resistance of 3D perovskite films. Investigating novel and stable charge transport layer and electrode materials is also of significance for the chemical stability of PSCs. Future molecular design of charge transport materials should consider the energy level alignment, high carrier mobility and stability. The cheap and chemically stable carbon electrode might be an alternative to reduce the cost and deterioration for lead halide PSCs. It's expected that rational management of interfacial chemical reactions in the whole PSCs will lead to substantial performance enhancement, paying the way for the commercialization of PSCs in the future.

References

1. A. Kojima, K. Teshima, Y. Shirai, T. Miyasaka, Organometal halide perovskites as visible-light sensitizers for photovoltaic cells. J. Am. Chem. Soc. **131**, 6050 (2009). https://doi.org/10.1021/ja809598r

2. J.-H. Im, C.-R. Lee, J.-W. Lee, S.-W. Park, N.-G. Park, 6.5% efficient perovskite quantum-dot-sensitized solar cell. Nanoscale **3**, 4088 (2011). https://doi.org/10.1039/C1NR10867K

3. M.M. Lee, J. Teuscher, T. Miyasaka, T.N. Murakami, H.J. Snaith, Efficient hybrid solar cells based on meso-superstructured organometal halide perovskites. Science **338**, 643 (2012). https://doi.org/10.1126/science.1228604

4. J.H. Heo, S.H. Im, J.H. Noh, T.N. Mandal, C.S. Lim et al., Efficient inorganic-organic hybrid heterojunction solar cells containing perovskite compound and polymeric hole conductors. Nat. Photonics **7**, 487 (2013). https://doi.org/10.1038/Nphoton.2013.80

5. H. Min, D.Y. Lee, J. Kim, G. Kim, K.S. Lee et al., Perovskite solar cells with atomically coherent interlayers on SnO_2 electrodes. Nature **598**, 444 (2021). https://doi.org/10.1038/s41586-021-03964-8

6. H.-S. Kim, C.-R. Lee, J.-H. Im, K.-B. Lee, T. Moehl et al., Lead iodide perovskite sensitized all-solid-state submicron thin film mesoscopic solar cell with efficiency exceeding 9%. Sci. Rep. **2**, 591 (2012). https://doi.org/10.1038/srep00591

7. C. Jiang, J. Zhou, H. Li, L. Tan, M. Li et al., Double layer composite electrode strategy for efficient perovskite solar cells with excellent reverse-bias stability. Nano-Micro Lett. **15**, 12 (2022). https://doi.org/10.1007/s40820-022-00985-4

8. W. Travis, E.N.K. Glover, H. Bronstein, D.O. Scanlon, R.G. Palgrave, On the application of the tolerance factor to inorganic and hybrid halide perovskites: a revised system. Chem. Sci. **7**, 4548 (2016). https://doi.org/10.1039/C5SC04845A

9. L. Qiu, S. He, L.K. Ono, Y. Qi, Progress of surface science studies on ABX_3-based metal halide perovskite solar cells. Adv. Energy Mater. **10**, 1902726 (2020). https://doi.org/10.1002/aenm.201902726

10. M. Anaya, G. Lozano, M.E. Calvo, H. Míguez, ABX_3 perovskites for tandem solar cells. Joule **1**, 769 (2017). https://doi.org/10.1016/j.joule.2017.09.017

11. C. Yi, J. Luo, S. Meloni, A. Boziki, N. Ashari-Astani et al., Entropic stabilization of mixed A-cation ABX_3 metal halide perovskites for high performance perovskite solar cells. Energy Environ. Sci. **9**, 656 (2016). https://doi.org/10.1039/C5EE03255E

12. S. Wang, T. Sakurai, W. Wen, Y. Qi, Energy level alignment at interfaces in metal halide perovskite solar cells. Adv. Mater. Interfaces **5**, 1800260 (2018). https://doi.org/10.1002/admi.201800260

13. L. Meng, J. You, T.-F. Guo, Y. Yang, Recent advances in the inverted planar structure of perovskite solar cells. Acc. Chem. Res. **49**, 155 (2016). https://doi.org/10.1021/acs.accounts.5b00404

14. Z. Liu, A. Zhu, F. Cai, L. Tao, Y. Zhou et al., Nickel oxide nanoparticles for efficient hole transport in p-i-n and n-i-p perovskite solar cells. J. Mater. Chem. A **5**, 6597 (2017). https://doi.org/10.1039/C7TA01593C

15. C. Momblona, L. Gil-Escrig, E. Bandiello, E.M. Hutter, M. Sessolo et al., Efficient vacuum deposited p-i-n and n-i-p perovskite solar cells employing doped charge transport layers. Energy Environ. Sci. **9**, 3456 (2016). https://doi.org/10.1039/C6EE02100J

16. Z. Zhang, J. Liang, J. Wang, Y. Zheng, X. Wu et al., Resolving mixed intermediate phases in methylammonium-free Sn–Pb alloyed perovskites for high-performance solar cells. Nano-Micro Lett. **14**, 165 (2022). https://doi.org/10.1007/s40820-022-00918-1

17. A. Polman, M. Knight, E.C. Garnett, B. Ehrler, W.C. Sinke, Photovoltaic materials: present efficiencies and future challenges. Science **352**, aad4424 (2016). https://doi.org/10.1126/science.aad4424

18. F. Huang, M. Li, P. Siffalovic, G. Cao, J. Tian, From scalable solution fabrication of perovskite films towards commercialization of solar cells. Energy Environ. Sci. **12**, 518 (2019). https://doi.org/10.1039/C8EE03025A

19. F. Yang, L. Dong, D. Jang, B. Saparov, K.C. Tam et al., Low temperature processed fully printed efficient planar structure carbon electrode perovskite solar cells and modules. Adv. Energy Mater. **11**, 2101219 (2021). https://doi.org/10.1002/aenm.202101219

20. A. Mei, X. Li, L. Liu, Z. Ku, T. Liu et al., A hole-conductor–free, fully printable mesoscopic perovskite solar cell with high stability. Science **345**, 295 (2014). https://doi.org/10.1126/science.1254763

21. H. Zhou, Q. Chen, G. Li, S. Luo, T.-B. Song et al., Interface engineering of highly efficient perovskite solar cells. Science **345**, 542 (2014). https://doi.org/10.1126/science.1254050

22. J.-P. Correa-Baena, M. Saliba, T. Buonassisi, M. Grätzel, A. Abate et al., Promises and challenges of perovskite solar cells. Science **358**, 739 (2017). https://doi.org/10.1126/science.aam6323

23. X. Lin, Y. Wang, H. Su, Z. Qin, Z. Zhang et al., An in-situ formed tunneling layer enriches the options of anode for efficient and stable regular perovskite solar cells. Nano-Micro Lett. **15**, 10 (2022). https://doi.org/10.1007/s40820-022-00975-6

24. I. Massiot, A. Cattoni, S. Collin, Progress and prospects for ultrathin solar cells. Nat. Energy **5**, 959 (2020). https://doi.org/10.1038/s41560-020-00714-4

25. M.A. Green, E.D. Dunlop, J. Hohl-Ebinger, M. Yoshita, N. Kopidakis et al., Solar cell efficiency tables (version 59). Prog. Photovolt. **30**, 3–12 (2022). https://doi.org/10.1002/pip.3506

26. Japan Electrical Safety & Environment Technology Laboratories, Chinese Perovskite Tech Firm Wuxi Utmost Light Claims 20.5% 'World Record' Efficiency For Perovskite Solar Mini Module, Certified By Japan's JET; Plans To Build Large Area Perovskite Solar Module Production Lines, http://taiyangnews.info/technology/20-5-world-record-efficiency-for-perovskite-solar-module/, 2021.

27. L. Fu, H. Li, L. Wang, R. Yin, B. Li et al., Defect passivation strategies in perovskites for an enhanced photovoltaic performance. Energy Environ. Sci. **13**, 4017 (2020). https://doi.org/10.1039/D0EE01767A

28. W.E.I. Sha, X. Ren, L. Chen, W.C.H. Choy, The efficiency limit of $CH_3NH_3PbI_3$ perovskite solar cells. Appl. Phys. Lett. **106**, 221104 (2015). https://doi.org/10.1063/1.4922150

29. S. Draguta, J.A. Christians, Y.V. Morozov, A. Mucunzi, J.S. Manser et al., A quantitative and spatially resolved analysis of the performance-bottleneck in high efficiency, planar hybrid perovskite solar cells. Energy Environ. Sci. **11**, 960 (2018). https://doi.org/10.1039/C7EE03654J

30. X. Ren, Z. Wang, W.E.I. Sha, W.C.H. Choy, Exploring the way to approach the efficiency limit of perovskite solar cells by drift-diffusion model. ACS Photonics **4**, 934 (2017). https://doi.org/10.1021/acsphotonics.6b01043

31. W.E.I. Sha, H. Zhang, Z.S. Wang, H.L. Zhu, X. Ren et al., Quantifying efficiency loss of perovskite solar cells by a modified detailed balance model. Adv. Energy Mater. **8**, 1701586 (2018). https://doi.org/10.1002/aenm.201701586

32. X. Zhao, N.-G. Park, Stability issues on perovskite solar cells. Photonics **2**, 1139 (2015). https://doi.org/10.3390/photonics2041139

33. A. Aftab, M.I. Ahmad, A review of stability and progress in tin halide perovskite solar cell. Sol. Energy **216**, 26 (2021). https://doi.org/10.1016/j.solener.2020.12.065

34. R. Wang, M. Mujahid, Y. Duan, Z.K. Wang, J. Xue et al., A review of perovskites solar cell stability. Adv. Funct. Mater. **29**, 1808843 (2019). https://doi.org/10.1002/adfm.201808843

35. J. Feng, X. Zhu, Z. Yang, X. Zhang, J. Niu et al., Record efficiency stable flexible perovskite solar cell using effective additive assistant strategy. Adv. Mater. **30**, 1801418 (2018). https://doi.org/10.1002/adma.201801418

36. M.M. Tavakoli, P. Yadav, R. Tavakoli, J. Kong, Surface engineering of TiO$_2$ ETL for highly efficient and hysteresis-less planar perovskite solar cell (21.4%) with enhanced open-circuit voltage and stability. Adv. Energy Mater. **8**, 1800794 (2018). https://doi.org/10.1002/aenm.201800794

37. L. Meng, J. You, Y. Yang, Addressing the stability issue of perovskite solar cells for commercial applications. Nat. Commun. **9**, 1 (2018). https://doi.org/10.1038/s41467-018-07255-1

38. N. Sultana, N.J. Demarais, D. Shevchenko, P.J. Derrick, Laser desorption/ionization mass spectrometry of perovskite solar cells: identification of interface interactions and degradation reactions. Sol. RRL **2**, 1800022 (2018). https://doi.org/10.1002/solr.201800022

39. J. Wei, Q. Wang, J. Huo, F. Gao, Z. Gan et al., Mechanisms and suppression of photoinduced degradation in perovskite solar cells. Adv. Energy Mater. **11**, 2002326 (2021). https://doi.org/10.1002/aenm.202002326

40. N. Li, X. Niu, Q. Chen, H. Zhou, Towards commercialization: the operational stability of perovskite solar cells. Chem. Soc. Rev. **49**, 8235 (2020). https://doi.org/10.1039/D0CS00573H

41. J. Wang, X. Chen, F. Jiang, Q. Luo, L. Zhang et al., Electrochemical corrosion of Ag electrode in the silver grid electrode-based flexible perovskite solar cells and the suppression method. Sol. RRL **2**, 1800118 (2018). https://doi.org/10.1002/solr.201800118

42. X. Wang, K. Rakstys, K. Jack, H. Jin, J. Lai et al., Engineering fluorinated-cation containing inverted perovskite solar cells with an efficiency of >21% and improved stability towards humidity. Nat. Commun. **12**, 52 (2021). https://doi.org/10.1038/s41467-020-20272-3

43. Z. Liu, L. Qiu, L.K. Ono, S. He, Z. Hu et al., A holistic approach to interface stabilization for efficient perovskite solar modules with over 2,000-hour operational stability. Nat. Energy **5**, 596 (2020). https://doi.org/10.1038/s41560-020-0653-2

44. S. Yang, S. Chen, E. Mosconi, Y. Fang, X. Xiao et al., Stabilizing halide perovskite surfaces for solar cell operation with wide-bandgap lead oxysalts. Science **365**, 473 (2019). https://doi.org/10.1126/science.aax3294

45. P. Hang, J. Xie, C. Kan, B. Li, Y. Zhang et al., Stabilizing fullerene for burn-in-free and stable perovskite solar cells under ultraviolet preconditioning and light soaking. Adv. Mater. **33**, 2006910 (2021). https://doi.org/10.1002/adma.202006910

46. Y. Rong, Y. Hu, A. Mei, H. Tan, M.I. Saidaminov et al., Challenges for commercializing perovskite solar cells. Science **361**, 8235 (2018). https://doi.org/10.1126/science.aat8235

47. X. Ma, L. Yang, X. Shang, M. Li, D. Gao et al., Grain boundary defect passivation by in situ formed wide-bandgap lead sulfate for efficient and stable perovskite solar cells. Chem.

Eng. J. **426**, 130685 (2021). https://doi.org/10.1016/j.cej.2021.130685

48. J.M. Frost, K.T. Butler, F. Brivio, C.H. Hendon, M. van Schilfgaarde et al., Atomistic origins of high-performance in hybrid halide perovskite solar cells. Nano Lett. **14**, 2584 (2014). https://doi.org/10.1021/nl500390f

49. J. Carrillo, A. Guerrero, S. Rahimnejad, O. Almora, I. Zarazua et al., Ionic reactivity at contacts and aging of methylammonium lead triiodide perovskite solar cells. Adv. Energy Mater. **6**, 1502246 (2016). https://doi.org/10.1002/aenm.201502246

50. J.A. Christians, P.A. MirandaHerrera, P.V. Kamat, Transformation of the excited state and photovoltaic efficiency of CH$_3$NH$_3$PbI$_3$ perovskite upon controlled exposure to humidified air. J. Am. Chem. Soc. **137**, 1530 (2015). https://doi.org/10.1021/ja511132a

51. A.M.A. Leguy, Y. Hu, M. Campoy-Quiles, M.I. Alonso, O.J. Weber et al., Reversible hydration of CH$_3$NH$_3$PbI$_3$ in films, single crystals, and solar cells. Chem. Mater. **27**, 3397 (2015). https://doi.org/10.1021/acs.chemmater.5b00660

52. G. Ren, W. Han, Q. Zhang, Z. Li, Y. Deng et al., Overcoming perovskite corrosion and de-doping through chemical binding of halogen bonds toward efficient and stable perovskite solar cells. Nano-Micro Lett. **14**, 175 (2022). https://doi.org/10.1007/s40820-022-00916-3

53. G. Tong, L.K. Ono, Y. Liu, H. Zhang, T. Bu et al., Up-scalable fabrication of SnO$_2$ with multifunctional interface for high performance perovskite solar modules. Nano-Micro Lett. **13**, 155 (2021). https://doi.org/10.1007/s40820-021-00675-7

54. T. Wu, Z. Qin, Y. Wang, Y. Wu, W. Chen et al., The main progress of perovskite solar cells in 2020–2021. Nano-Micro Lett. **13**, 152 (2021). https://doi.org/10.1007/s40820-021-00672-w

55. Z. Li, Y. Gao, Z. Zhang, Q. Xiong, L. Deng et al., cPCN-regulated SnO$_2$ composites enables perovskite solar cell with efficiency beyond 23%. Nano-Micro Lett. **13**, 101 (2021). https://doi.org/10.1007/s40820-021-00636-0

56. D. Bryant, N. Aristidou, S. Pont, I. Sanchez-Molina, T. Chotchuangchutchaval et al., Light and oxygen induced degradation limits the operational stability of methylammonium lead triiodide perovskite solar cells. Energy Environ. Sci. **9**, 1850 (2016). https://doi.org/10.1039/c6ee90023b

57. D. Bryant, N. Aristidou, S. Pont, I. Sanchez-Molina, T. Chotchunangatchaval et al., Light and oxygen induced degradation limits the operational stability of methylammonium lead triiodide perovskite solar cells. Energy Environ. Sci. **9**, 1655 (2016). https://doi.org/10.1039/C6EE00409A

58. W. Chi, S.K. Banerjee, Achieving resistance against moisture and oxygen for perovskite solar cells with high efficiency and stability. Chem. Mater. **33**, 4269–4303 (2021). https://doi.org/10.1021/acs.chemmater.1c00773

59. G. Niu, X. Guo, L. Wang, Review of recent progress in chemical stability of perovskite solar cells. J. Mater. Chem. A **3**, 8970 (2015). https://doi.org/10.1039/C4TA04994B

60. F. Li, M. Liu, Recent efficient strategies for improving the moisture stability of perovskite solar cells. J. Mater. Chem. A **5**, 15447 (2017). https://doi.org/10.1039/C7TA01325F

61. J. Jiang, Q. Wang, Z. Jin, X. Zhang, J. Lei et al., Polymer doping for high-efficiency perovskite solar cells with improved moisture stability. Adv. Energy Mater. **8**, 1701757 (2018). https://doi.org/10.1002/aenm.201701757

62. I. Hwang, I. Jeong, J. Lee, M.J. Ko, K. Yong, Enhancing stability of perovskite solar cells to moisture by the facile hydrophobic passivation. ACS Appl. Mater. Interfaces **7**, 17330 (2015). https://doi.org/10.1021/acsami.5b04490

63. J. Yang, B.D. Siempelkamp, D. Liu, T.L. Kelly, Investigation of $CH_3NH_3PbI_3$ degradation rates and mechanisms in controlled humidity environments using in situ techniques. ACS Nano **9**, 1955 (2015). https://doi.org/10.1021/nn506864k

64. J. Zhu, D.H. Kim, J.D. Kim, D.G. Lee, W.B. Kim et al., All-in-one Lewis base for enhanced precursor and device stability in highly efficient perovskite solar cells. ACS Energy Lett. **6**, 3425 (2021). https://doi.org/10.1021/acsenergylett.1c01465

65. L. Yu, T. Guo, H. Yuan, Z. Zhang, Z. Deng et al., Effective lewis base additive with S-donor for efficient and stable $CsPbI_2Br$ based perovskite solar cells. Chem. Eng. J. **420**, 129931 (2021). https://doi.org/10.1016/j.cej.2021.129931

66. W. Xiang, S. Liu, W. Tress, A review on the stability of inorganic metal halide perovskites: challenges and opportunities for stable solar cells. Energy Environ. Sci. **14**, 2090 (2021). https://doi.org/10.1039/D1EE00157D

67. S. Xiong, M. Yuan, J. Yang, J. Song, X. Guo et al., Engineering of the back contact between PCBM and metal electrode for planar perovskite solar cells with enhanced efficiency and stability. Adv. Opt. Mater. **7**, 1900542 (2019). https://doi.org/10.1002/adom.201900542

68. B. Rivkin, P. Fassl, Q. Sun, A.D. Taylor, Z. Chen et al., Effect of ion migration-induced electrode degradation on the operational stability of perovskite solar cells. ACS Omega **3**, 10042 (2018). https://doi.org/10.1021/acsomega.8b01626

69. Z. Yang, B.H. Babu, S. Wu, T. Liu, S. Fang et al., Review on practical interface engineering of perovskite solar cells: from efficiency to stability. Sol. RRL **4**, 1900257 (2020). https://doi.org/10.1002/solr.201900257

70. Y. Xu, Z. Lin, W. Wei, Y. Hao, S. Liu et al., Recent progress of electrode materials for flexible perovskite solar cells. Nano-Micro Lett. **14**, 117 (2022). https://doi.org/10.1007/s40820-022-00859-9

71. K.M.M. Salim, S. Masi, A.F. Gualdrón-Reyes, R.S. Sánchez, E.M. Barea et al., Boosting long-term stability of pure formamidinium perovskite solar cells by ambient air additive assisted fabrication. ACS Energy Lett. **6**, 3511 (2021). https://doi.org/10.1021/acsenergylett.1c01311

72. H. Zheng, X. Xu, S. Xu, G. Liu, S. Chen et al., The multiple effects of polyaniline additive to improve the efficiency and stability of perovskite solar cells. J. Mater. Chem. C **7**, 4441 (2019). https://doi.org/10.1039/C8TC05975F

73. L. Xie, J. Chen, P. Vashishtha, X. Zhao, G.S. Shin et al., Importance of functional groups in cross-linking methoxysilane additives for high-efficiency and stable perovskite solar cells. ACS Energy Lett. **4**, 2192 (2019). https://doi.org/10.1021/acsenergylett.9b01356

74. C. Park, H. Ko, D.H. Sin, K.C. Song, K. Cho, Organometal halide perovskite solar cells with improved thermal stability via grain boundary passivation using a molecular additive. Adv. Funct. Mater. **27**, 1703546 (2017). https://doi.org/10.1002/adfm.201703546

75. Y. Chen, X. Yang, P. Liu, W. Wang, R. Ran et al., Improving moisture/thermal stability and efficiency of $CH_3NH_3PbI_3$-based perovskite solar cells via gentle butyl acrylate additive strategy. Sol. RRL **5**, 2000621 (2021). https://doi.org/10.1002/solr.202000621

76. J. Xu, J. Cui, S. Yang, Y. Han, X. Guo et al., Unraveling passivation mechanism of imidazolium-based ionic liquids on inorganic perovskite to achieve near-record-efficiency $CsPbI_2Br$ solar cells. Nano-Micro Lett. **14**, 7 (2021). https://doi.org/10.1007/s40820-021-00763-8

77. W. Zhao, J. Xu, K. He, Y. Cai, Y. Han et al., A special additive enables all cations and anions passivation for stable perovskite solar cells with efficiency over 23%. Nano-Micro Lett. **13**, 169 (2021). https://doi.org/10.1007/s40820-021-00688-2

78. S. Tang, Y. Deng, X. Zheng, Y. Bai, Y. Fang et al., Composition engineering in doctor-blading of perovskite solar cells. Adv. Energy Mater. **7**, 1700302 (2017). https://doi.org/10.1002/aenm.201700302

79. Y. Jiang, X. He, T. Liu, N. Zhao, M. Qin et al., Intralayer a-site compositional engineering of ruddlesden–popper perovskites for thermostable and efficient solar cells. ACS Energy Lett. **4**, 1216 (2019). https://doi.org/10.1021/acsenergylett.9b00403

80. T. Ozturk, E. Akman, A.E. Shalan, S. Akin, Composition engineering of operationally stable $CsPbI_2Br$ perovskite solar cells with a record efficiency over 17%. Nano Energy **87**, 106157 (2021). https://doi.org/10.1016/j.nanoen.2021.106157

81. X. Jin, L. Yang, X.-F. Wang, Efficient two-dimensional perovskite solar cells realized by incorporation of Ti_3C_2Tx MXene as nano-dopants. Nanomicro. Lett. **13**, 68 (2021). https://doi.org/10.1007/s40820-021-00602-w

82. J. Liu, S.K. Pathak, N. Sakai, R. Sheng, S. Bai et al., Identification and mitigation of a critical interfacial instability in perovskite solar cells employing copper thiocyanate hole-transporter. Adv. Mater. Interfaces **3**, 1600571 (2016). https://doi.org/10.1002/admi.201600571

83. J. Zhang, J. Long, Z. Huang, J. Yang, X. Li et al., Obstructing interfacial reaction between NiO_x and perovskite to enable efficient and stable inverted perovskite solar cells. Chem. Eng. J. **426**, 131357 (2021). https://doi.org/10.1016/j.cej.2021.131357

84. S. Guarnera, A. Abate, W. Zhang, J.M. Foster, G. Richardson et al., Improving the long-term stability of perovskite solar cells with a porous Al_2O_3 buffer layer. J. Phys. Chem. Lett. **6**, 432 (2015). https://doi.org/10.1021/jz502703p

85. A. Capasso, F. Matteocci, L. Najafi, M. Prato, J. Buha et al., Few-layer MoS_2 flakes as active buffer layer for stable

perovskite solar cells. Adv. Energy Mater. **6**, 1600920 (2016). https://doi.org/10.1002/aenm.201600920

86. X. Zheng, H. Lei, G. Yang, W. Ke, Z. Chen et al., Enhancing efficiency and stability of perovskite solar cells via a high mobility p-type PbS buffer layer. Nano Energy **38**, 1 (2017). https://doi.org/10.1016/j.nanoen.2017.05.040

87. K. Chatzimanolis, K. Rogdakis, D. Tsikritzis, N. Tzoganakis, M. Tountas et al., Inverted perovskite solar cells with enhanced lifetime and thermal stability enabled by a metallic tantalum disulfide buffer layer. Nanoscale Adv. **3**, 3124 (2021). https://doi.org/10.1039/D1NA00172H

88. H. Zhong, W. Li, Y. Huang, D. Cao, C. Zhang et al., All-inorganic perovskite solar cells with tetrabutylammonium acetate as the buffer layer between the SnO_2 electron transport film and $CsPbI_3$. ACS Appl. Mater. Interfaces **14**, 5183 (2022). https://doi.org/10.1021/acsami.1c18375

89. W. Dong, W. Qiao, S. Xiong, J. Yang, X. Wang et al., Surface passivation and energetic modification suppress nonradiative recombination in perovskite solar cells. Nano-Micro Lett. **14**, 108 (2022). https://doi.org/10.1007/s40820-022-00854-0

90. L. Zhu, C. Chen, Y. Weng, F. Li, Q. Lou, Enhancing the performance of inverted perovskite solar cells by inserting a ZnO:TIPD film between PCBM layer and Ag electrode. Sol. Energy Mater. Sol. Cells **198**, 11 (2019). https://doi.org/10.1016/j.solmat.2019.04.007

91. C.-Y. Chang, C.-C. Wang, Enhanced stability and performance of air-processed perovskite solar cells via defect passivation with a thiazole-bridged diketopyrrolopyrrole-based π-conjugated polymer. J. Mater. Chem. A **8**, 8593 (2020). https://doi.org/10.1039/D0TA00978D

92. J. Chen, L. Zuo, Y. Zhang, X. Lian, W. Fu et al., High-performance thickness insensitive perovskite solar cells with enhanced moisture stability. Adv. Energy Mater. **8**, 1800438 (2018). https://doi.org/10.1002/aenm.201800438

93. Y. Han, S. Meyer, Y. Dkhissi, K. Weber, J.M. Pringle et al., Degradation observations of encapsulated planar $CH_3NH_3PbI_3$ perovskite solar cells at high temperatures and humidity. J. Mater. Chem. A **3**, 8139 (2015). https://doi.org/10.1039/C5TA00358J

94. G. Niu, W. Li, F. Meng, L. Wang, H. Dong et al., Study on the stability of CH3NH3PbI3 films and the effect of post-modification by aluminum oxide in all-solid-state hybrid solar cells. J. Mater. Chem. A **2**, 705 (2014). https://doi.org/10.1039/C3TA13606J

95. Q. Wang, B. Chen, Y. Liu, Y. Deng, Y. Bai et al., Scaling behavior of moisture-induced grain degradation in polycrystalline hybrid perovskite thin films. Energy Environ. Sci. **10**, 516 (2017). https://doi.org/10.1039/C6EE02941H

96. W. Huang, J.S. Manser, P.V. Kamat, S. Ptasinska, Evolution of chemical composition, morphology, and photovoltaic efficiency of $CH_3NH_3PbI_3$ perovskite under ambient conditions. Chem. Mater. **28**, 303 (2016). https://doi.org/10.1021/acs.chemmater.5b04122

97. N. Ahn, K. Kwak, M.S. Jang, H. Yoon, B.Y. Lee et al., Trapped charge-driven degradation of perovskite solar cells. Nat. Commun. **7**, 13422 (2016). https://doi.org/10.1038/ncomms13422

98. A.J. Pearson, G.E. Eperon, P.E. Hopkinson, S.N. Habisreutinger, J.T.-W. Wang et al., Oxygen degradation in mesoporous $Al_2O_3/CH_3NH_3PbI_{3-x}Cl_x$ perovskite solar cells: kinetics and mechanisms. Adv. Energy Mater. **6**, 1600014 (2016). https://doi.org/10.1002/aenm.201600014

99. L. Zhang, P.H.L. Sit, Ab initio study of the role of oxygen and excess electrons in the degradation of $CH_3NH_3PbI_3$. J. Mater. Chem. A **5**, 9042 (2017). https://doi.org/10.1039/C7TA01091E

100. N. Aristidou, I. Sanchez-Molina, T. Chotchuangchutchaval, M. Brown, L. Martinez et al., The role of oxygen in the degradation of methylammonium lead trihalide perovskite photoactive layers. Angew. Chem. Int. Ed. **54**, 8208 (2015). https://doi.org/10.1002/anie.201503153

101. N. Aristidou, C. Eames, I. Sanchez-Molina, X. Bu, J. Kosco et al., Fast oxygen diffusion and iodide defects mediate oxygen-induced degradation of perovskite solar cells. Nat. Commun. **8**, 15218 (2017). https://doi.org/10.1038/ncomms15218

102. J.S.W. Godding, A.J. Ramadan, Y.-H. Lin, K. Schutt, H.J. Snaith et al., Oxidative passivation of metal halide perovskites. Joule **3**, 2716 (2019). https://doi.org/10.1016/j.joule.2019.08.006

103. F. Lang, O. Shargaieva, V.V. Brus, H.C. Neitzert, J. Rappich et al., Influence of radiation on the properties and the stability of hybrid perovskites. Adv. Mater. **30**, 1702905 (2018). https://doi.org/10.1002/adma.201702905

104. T.D. Siegler, W.A. Dunlap-Shohl, Y. Meng, Y. Yang, W.F. Kau et al., Water-accelerated photooxidation of $CH_3NH_3PbI_3$ perovskite. J. Am. Chem. Soc. **144**, 5552 (2022). https://doi.org/10.1021/jacs.2c00391

105. A.J. Ramadan, L.A. Rochford, S. Fearn, H.J. Snaith, Processing solvent-dependent electronic and structural properties of cesium lead triiodide thin films. J. Phys. Chem. Lett. **8**, 4172 (2017). https://doi.org/10.1021/acs.jpclett.7b01677

106. Q. Sun, P. Fassl, D. Becker-Koch, A. Bausch, B. Rivkin et al., Role of microstructure in oxygen induced photodegradation of methylammonium lead triiodide perovskite films. Adv. Energy Mater. **7**, 1700977 (2017). https://doi.org/10.1002/aenm.201700977

107. Y. Ouyang, Y. Li, P. Zhu, Q. Li, Y. Gao et al., Photo-oxidative degradation of methylammonium lead iodide perovskite: mechanism and protection. J. Mater. Chem. A **7**, 2275 (2019). https://doi.org/10.1039/C8TA12193A

108. W. Li, W. Zhang, S. Van Reenen, R.J. Sutton, J. Fan et al., Enhanced UV-light stability of planar heterojunction perovskite solar cells with caesium bromide interface modification. Energy Environ. Sci. **9**, 490 (2016). https://doi.org/10.1039/C5EE03522H

109. T. Leijtens, G.E. Eperon, S. Pathak, A. Abate, M.M. Lee et al., Overcoming ultraviolet light instability of sensitized TiO_2 with meso-superstructured organometal tri-halide perovskite solar cells. Nat. Commun. **4**, 2885 (2013). https://doi.org/10.1038/ncomms3885

110. Y. Li, X. Xu, C. Wang, B. Ecker, J. Yang et al., Light-induced degradation of $CH_3NH_3PbI_3$ hybrid perovskite thin film. J. Phys. Chem. C **121**, 3904 (2017). https://doi.org/10.1021/acs.jpcc.6b11853

111. Z. Song, C. Wang, A.B. Phillips, C.R. Grice, D. Zhao et al., Probing the origins of photodegradation in organic–inorganic metal halide perovskites with time-resolved mass spectrometry. Sustain. Energy Fuels **2**, 2460 (2018). https://doi.org/10.1039/C8SE00358K

112. S.G. Motti, D. Meggiolaro, A.J. Barker, E. Mosconi, C.A.R. Perini et al., Controlling competing photochemical reactions stabilizes perovskite solar cells. Nat. Photonics **13**, 532–539 (2019). https://doi.org/10.1038/s41566-019-0435-1

113. J.M. Azpiroz, E. Mosconi, J. Bisquert, F. De Angelis, Defect migration in methylammonium lead iodide and its role in perovskite solar cell operation. Energy Environ. Sci. **8**, 2118 (2015). https://doi.org/10.1039/C5EE01265A

114. R. Gottesman, E. Haltzi, L. Gouda, S. Tirosh, Y. Bouhadana et al., Extremely slow photoconductivity response of $CH_3NH_3PbI_3$ perovskites suggesting structural changes under working conditions. J. Phys. Chem. Lett. **5**, 2662 (2014). https://doi.org/10.1021/jz501373f

115. Y. You, W. Tian, L. Min, F. Cao, K. Deng et al., TiO_2/WO_3 bilayer as electron transport layer for efficient planar perovskite solar cell with efficiency exceeding 20%. Adv. Mater. Interfaces **7**, 1901406 (2020). https://doi.org/10.1002/admi.201901406

116. M.M. Byranvand, T. Kim, S. Song, G. Kang, S.U. Ryu et al., p-type CuI islands on TiO_2 electron transport layer for a highly efficient planar-perovskite solar cell with negligible hysteresis. Adv. Energy Mater. **8**, 1702235 (2018). https://doi.org/10.1002/aenm.201702235

117. M. Kim, I.-W. Choi, S.J. Choi, J.W. Song, S.-I. Mo et al., Enhanced electrical properties of Li-salts doped mesoporous TiO_2 in perovskite solar cells. Joule **5**, 659 (2021). https://doi.org/10.1016/j.joule.2021.02.007

118. B. Wang, J. Yang, L. Lu, W. Xiao, H. Wu et al., Interface engineering of air-stable n-doping fullerene-modified TiO_2 electron transport layer for highly efficient and stable perovskite solar cells. Adv. Mater. Interfaces **7**, 1901964 (2020). https://doi.org/10.1002/admi.201901964

119. S. Haque, M.J. Mendes, O. Sanchez-Sobrado, H. Águas, E. Fortunato et al., Photonic-structured TiO_2 for high-efficiency, flexible and stable perovskite solar cells. Nano Energy **59**, 91 (2019). https://doi.org/10.1016/j.nanoen.2019.02.023

120. T. Leijtens, G.E. Eperon, S. Pathak, A. Abate, M.M. Lee et al., Overcoming ultraviolet light instability of sensitized TiO_2 with meso-superstructured organometal tri-halide perovskite solar cells. Nat. Commun. **4**, 1 (2013). https://doi.org/10.1038/ncomms3885

121. M. Shahiduzzaman, M.I. Hossain, S. Visal, T. Kaneko, W. Qarony et al., Spray pyrolyzed TiO_2 embedded multi-layer front contact design for high-efficiency perovskite solar cells. Nano-Micro. Lett. **13**, 36 (2021). https://doi.org/10.1007/s40820-020-00559-2

122. V. Roiati, E. Mosconi, A. Listorti, S. Colella, G. Gigli et al., Stark effect in perovskite/TiO_2 solar cells: evidence of local interfacial order. Nano Lett. **14**, 2168 (2014). https://doi.org/10.1021/nl500544c

123. R.A. Kerner, B.P. Rand, Linking chemistry at the TiO_2/$CH_3NH_3PbI_3$ interface to current–voltage hysteresis. J. Phys. Chem. Lett. **8**, 2298 (2017). https://doi.org/10.1021/acs.jpclett.7b00712

124. S. Ito, S. Tanaka, K. Manabe, H. Nishino, Effects of surface blocking layer of Sb_2S_3 on nanocrystalline TiO_2 for $CH_3NH_3PbI_3$ perovskite solar cells. J. Phys. Chem. C **118**, 16995 (2014). https://doi.org/10.1021/jp500449z

125. J. Zhang, T. Pauporté, Effects of oxide contact layer on the preparation and properties of $CH_3NH_3PbI_3$ for perovskite solar cell application. J. Phys. Chem. C **119**, 14919 (2015). https://doi.org/10.1021/acs.jpcc.5b02984

126. M.M. Tavakoli, R. Tavakoli, Z. Nourbakhsh, A. Waleed, U.S. Virk et al., High efficiency and stable perovskite solar cell using ZnO/rGO QDs as an electron transfer layer. Adv. Mater. Interfaces **3**, 1500790 (2016). https://doi.org/10.1002/admi.201500790

127. H. Si, Q. Liao, Z. Zhang, Y. Li, X. Yang et al., An innovative design of perovskite solar cells with Al_2O_3 inserting at ZnO/perovskite interface for improving the performance and stability. Nano Energy **22**, 223 (2016). https://doi.org/10.1016/j.nanoen.2016.02.025

128. R. Azmi, S. Hwang, W. Yin, T.-W. Kim, T.K. Ahn et al., High efficiency low-temperature processed perovskite solar cells integrated with alkali metal doped ZnO electron transport layers. ACS Energy Lett. **3**, 1241 (2018). https://doi.org/10.1021/acsenergylett.8b00493

129. Z. Wang, X. Zhu, J. Feng, C. Wang, C. Zhang et al., Antisolvent-and annealing-free deposition for highly stable efficient perovskite solar cells via modified ZnO. Adv. Sci. **8**, 2002860 (2021). https://doi.org/10.1002/advs.202002860

130. J. Idígoras, A. Todinova, J.R. Sánchez-Valencia, A. Barranco, A. Borrás et al., The interaction between hybrid organic–inorganic halide perovskite and selective contacts in perovskite solar cells: an infrared spectroscopy study. Phys. Chem. Chem. Phys. **18**, 13583 (2016). https://doi.org/10.1039/C6CP01265E

131. J. Yang, B.D. Siempelkamp, E. Mosconi, F. De Angelis, T.L. Kelly, Origin of the thermal instability in $CH_3NH_3PbI_3$ thin films deposited on ZnO. Chem. Mater. **27**, 4229 (2015). https://doi.org/10.1021/acs.chemmater.5b01598

132. Y. Cheng, Q.-D. Yang, J. Xiao, Q. Xue, H.-W. Li et al., Decomposition of organometal halide perovskite films on zinc oxide nanoparticles. ACS Appl. Mater. Interfaces **7**, 36 (2015). https://doi.org/10.1021/acsami.5b04695

133. F. Hao, C.C. Stoumpos, D.H. Cao, R.P.H. Chang, M.G. Kanatzidis, Lead-free solid-state organic–inorganic halide perovskite solar cells. Nat. Photonics **8**, 489 (2014). https://doi.org/10.1038/nphoton.2014.82

134. F. Giustino, H.J. Snaith, Toward lead-free perovskite solar cells. ACS Energy Lett. **1**, 1233 (2016). https://doi.org/10.1021/acsenergylett.6b00499

135. Z. Li, L. Wang, R. Liu, Y. Fan, H. Meng et al., Spontaneous interface ion exchange: passivating surface defects of perovskite solar cells with enhanced photovoltage. Adv. Energy Mater. **9**, 1902142 (2019). https://doi.org/10.1002/aenm.201902142

136. J. You, L. Meng, T.-B. Song, T.-F. Guo, Y. Yang et al., Improved air stability of perovskite solar cells via solution-processed metal oxide transport layers. Nat. Nanotechnol. **11**, 75 (2016). https://doi.org/10.1038/nnano.2015.230

137. H. Lee, C. Lee, Analysis of ion-diffusion-induced interface degradation in inverted perovskite solar cells via restoration of the Ag electrode. Adv. Energy Mater. **8**, 1702197 (2018). https://doi.org/10.1002/aenm.201702197

138. J. Xu, A. Buin, A.H. Ip, W. Li, O. Voznyy et al., Perovskite–fullerene hybrid materials suppress hysteresis in planar diodes. Nat. Commun. **6**, 7081 (2015). https://doi.org/10.1038/ncomms8081

139. Q. Wang, C.-C. Chueh, M. Eslamian, A.K.-Y. Jen, Modulation of PEDOT: PSS pH for efficient inverted perovskite solar cells with reduced potential loss and enhanced stability. ACS Appl. Mater. Interfaces **8**, 32068 (2016). https://doi.org/10.1021/acsami.6b11757

140. W. Sun, Y. Li, Y. Xiao, Z. Zhao, S. Ye et al., An ammonia modified PEDOT: PSS for interfacial engineering in inverted planar perovskite solar cells. Org. Electron. **46**, 22 (2017). https://doi.org/10.1016/j.orgel.2017.03.019

141. Y. Jiang, S.-C. Yang, Q. Jeangros, S. Pisoni, T. Moser et al., Mitigation of vacuum and illumination-induced degradation in perovskite solar cells by structure engineering. Joule **4**, 1087 (2020). https://doi.org/10.1016/j.joule.2020.03.017

142. Y. Li, B. Wang, T. Liu, Q. Zeng, D. Cao et al., Interfacial engineering of PTAA/perovskites for improved crystallinity and hole extraction in inverted perovskite solar cells. ACS Appl. Mater. Interfaces **14**, 3284 (2022). https://doi.org/10.1021/acsami.1c21000

143. T. Liu, K. Chen, Q. Hu, R. Zhu, Q. Gong, Inverted perovskite solar cells: progresses and perspectives. Adv. Energy Mater. **6**, 1600457 (2016). https://doi.org/10.1002/aenm.201600457

144. H. Wang, Z. Huang, S. Xiao, X. Meng, Z. Xing et al., An in situ bifacial passivation strategy for flexible perovskite solar module with mechanical robustness by roll-to-roll fabrication. J. Mater. Chem. A **9**, 5759 (2021). https://doi.org/10.1039/D0TA12067G

145. M. Du, S. Zhao, L. Duan, Y. Cao, H. Wang et al., Surface redox engineering of vacuum-deposited NiOx for top-performance perovskite solar cells and modules. Joule **6**, 1931 (2022). https://doi.org/10.1016/j.joule.2022.06.026

146. W. Chen, F.Z. Liu, X.Y. Feng, A.B. Djurišić, W.K. Chan et al., Cesium doped NiOx as an efficient hole extraction layer for inverted planar perovskite solar cells. Adv. Energy Mater. **7**, 1700722 (2017). https://doi.org/10.1002/aenm.201700722

147. J.R. Manders, S.W. Tsang, M.J. Hartel, T.H. Lai, S. Chen et al., Solution-processed nickel oxide hole transport layers in high efficiency polymer photovoltaic cells. Adv. Funct. Mater. **23**, 2993 (2013). https://doi.org/10.1002/adfm.201202269

148. C.C. Boyd, R.C. Shallcross, T. Moot, R. Kerner, L. Bertoluzzi et al., Overcoming redox reactions at perovskite-nickel oxide interfaces to boost voltages in perovskite solar cells. Joule **4**, 1759 (2020). https://doi.org/10.1016/j.joule.2020.06.004

149. F. Hou, Z. Su, F. Jin, X. Yan, L. Wang et al., Efficient and stable planar heterojunction perovskite solar cells with an MoO$_3$/PEDOT: PSS hole transporting layer. Nanoscale **7**, 9427 (2015). https://doi.org/10.1039/C5NR01864A

150. J.W. Jo, M.S. Seo, M. Park, J.Y. Kim, J.S. Park et al., Improving performance and stability of flexible planar-heterojunction perovskite solar cells using polymeric hole-transport material. Adv. Funct. Mater. **26**, 4464 (2016). https://doi.org/10.1002/adfm.201600746

151. Y. Meng, Z. Hu, N. Ai, Z. Jiang, J. Wang et al., Improving the stability of bulk heterojunction solar cells by incorporating pH-neutral PEDOT: PSS as the hole transport layer. ACS Appl. Mater. Interfaces **6**, 5122 (2014). https://doi.org/10.1021/am500336s

152. C. Redondo-Obispo, T.S. Ripolles, S. Cortijo-Campos, A.L. Alvarez, E. Climent-Pascual et al., Enhanced stability and efficiency in inverted perovskite solar cells through graphene doping of PEDOT: PSS hole transport layer. Mater. Design. **191**, 108587 (2020). https://doi.org/10.1016/j.matdes.2020.108587

153. C. Liu, L. Zhang, Y. Li, X. Zhou, S. She et al., Highly stable and efficient perovskite solar cells with 22.0% efficiency based on inorganic–organic dopant-free double hole transporting layers. Adv. Funct. Mater. **30**, 1908462 (2020). https://doi.org/10.1002/adfm.201908462

154. S. Kim, S. Bae, S.-W. Lee, K. Cho, K.D. Lee et al., Relationship between ion migration and interfacial degradation of CH$_3$NH$_3$PbI$_3$ perovskite solar cells under thermal conditions. Sci. Rep. **7**, 1 (2017). https://doi.org/10.1038/s41598-017-00866-6

155. T. Wu, R. Zhuang, R. Zhao, R. Zhao, L. Zhu et al., Understanding the effects of fluorine substitution in lithium salt on photovoltaic properties and stability of perovskite solar cells. ACS Energy Lett. **6**, 2218–2228 (2021). https://doi.org/10.1021/acsenergylett.1c00685

156. Y. Liu, Y. Hu, X. Zhang, P. Zeng, F. Li et al., Inhibited aggregation of lithium salt in spiro-OMeTAD toward highly efficient perovskite solar cells. Nano Energy **70**, 104483 (2020). https://doi.org/10.1016/j.nanoen.2020.104483

157. W. Li, H. Dong, L. Wang, N. Li, X. Guo et al., Montmorillonite as bifunctional buffer layer material for hybrid perovskite solar cells with protection from corrosion and retarding recombination. J. Mater. Chem. A **2**, 13587 (2014). https://doi.org/10.1039/C4TA01550A

158. Y. Yue, N. Salim, Y. Wu, X. Yang, A. Islam et al., Enhanced stability of perovskite solar cells through corrosion-free pyridine derivatives in hole-transporting materials. Adv. Mater. **28**, 10738 (2016). https://doi.org/10.1002/adma.201602822

159. B.-A. Chen, J.-T. Lin, N.-T. Suen, C.-W. Tsao, T.-C. Chu et al., In situ identification of photo- and moisture-dependent

phase evolution of perovskite solar cells. ACS Energy Lett. **2**, 342 (2017). https://doi.org/10.1021/acsenergylett.6b00698

160. Q. Wu, C. Xue, Y. Li, P. Zhou, W. Liu et al., Kesterite Cu_2ZnSnS_4 as a low-cost inorganic hole-transporting material for high-efficiency perovskite solar cells. ACS Appl. Mater. Interfaces **7**, 28466 (2015). https://doi.org/10.1021/acsami.5b09572

161. Y. Yang, H. Chen, X. Zheng, X. Meng, T. Zhang et al., Ultrasound-spray deposition of multi-walled carbon nanotubes on NiO nanoparticles-embedded perovskite layers for high-performance carbon-based perovskite solar cells. Nano Energy **42**, 322 (2017). https://doi.org/10.1016/j.nanoen.2017.11.003

162. C. Liu, X. Zhou, S. Chen, X. Zhao, S. Dai et al., Hydrophobic Cu_2O quantum dots enabled by surfactant modification as top hole-transport materials for efficient perovskite solar cells. Adv. Sci. **6**, 1801169 (2019). https://doi.org/10.1002/advs.201801169

163. I.S. Yang, S. Lee, J. Choi, M.T. Jung, J. Kim et al., Enhancement of open circuit voltage for CuSCN-based perovskite solar cells by controlling the perovskite/CuSCN interface with functional molecules. J. Mater. Chem. A **7**, 6028 (2019). https://doi.org/10.1039/C8TA12217B

164. B. Lee, A.J. Yun, J. Kim, B. Gil, B. Shin et al., Aminosilane-modified $CuGaO_2$ nanoparticles incorporated with CuSCN as a hole-transport layer for efficient and stable perovskite solar cells. Adv. Mater. Interfaces **6**, 1901372 (2019). https://doi.org/10.1002/admi.201901372

165. N. Arora, M.I. Dar, A. Hinderhofer, N. Pellet, F. Schreiber et al., Perovskite solar cells with CuSCN hole extraction layers yield stabilized efficiencies greater than 20%. Science **358**, 768 (2017). https://doi.org/10.1126/science.aam5655

166. G.A. Sepalage, S. Meyer, A.R. Pascoe, A.D. Scully, U. Bach et al., A facile deposition method for CuSCN: exploring the influence of CuSCN on JV hysteresis in planar perovskite solar cells. Nano Energy **32**, 310 (2017). https://doi.org/10.1016/j.nanoen.2016.12.043

167. P. Xu, J. Liu, J. Huang, F. Yu, C.-H. Li et al., Interfacial engineering of CuSCN-based perovskite solar cells via PMMA interlayer toward enhanced efficiency and stability. New J. Chem. **45**, 13168 (2021). https://doi.org/10.1039/D1NJ02454J

168. L. Kavan, Z.V. Živcová, P. Hubík, N. Arora, M.I. Dar et al., Electrochemical characterization of CuSCN hole-extracting thin films for perovskite photovoltaics. ACS Appl. Energy Mater. **2**, 4264 (2019). https://doi.org/10.1021/acsaem.9b00496

169. H.-S. Kim, I.-H. Jang, N. Ahn, M. Choi, A. Guerrero et al., Control of I-V hysteresis in $CH_3NH_3PbI_3$ perovskite solar cell. J. Phys. Chem. Lett. **6**, 4633 (2015). https://doi.org/10.1021/acs.jpclett.5b02273

170. T. Zhang, X. Meng, Y. Bai, S. Xiao, C. Hu et al., Profiling the organic cation-dependent degradation of organolead halide perovskite solar cells. J. Mater. Chem. A **5**, 1103 (2017). https://doi.org/10.1039/C6TA09687E

171. Y. Kato, L.K. Ono, M.V. Lee, S. Wang, S.R. Raga et al., Silver iodide formation in methyl ammonium lead iodide perovskite solar cells with silver top electrodes. Adv. Mater. Interfaces **2**, 1500195 (2015). https://doi.org/10.1002/admi.201500195

172. J. Li, Q. Dong, N. Li, L. Wang, Direct evidence of ion diffusion for the silver-electrode-induced thermal degradation of inverted perovskite solar cells. Adv. Energy Mater. **7**, 1602922 (2017). https://doi.org/10.1002/aenm.201602922

173. E. Lee, J. Ahn, H.C. Kwon, S. Ma, K. Kim et al., All-solution-processed silver nanowire window electrode-based flexible perovskite solar cells enabled with amorphous metal oxide protection. Adv. Energy Mater. **8**, 1702182 (2018). https://doi.org/10.1002/aenm.201702182

174. Y. Cheng, X. Liu, Z. Guan, M. Li, Z. Zeng et al., Revealing the degradation and self-healing mechanisms in perovskite solar cells by sub-bandgap external quantum efficiency spectroscopy. Adv. Mater. **33**, 2006170 (2021). https://doi.org/10.1002/adma.202006170

175. C.C. Boyd, R. Cheacharoen, K.A. Bush, R. Prasanna, T. Leijtens et al., Barrier design to prevent metal-induced degradation and improve thermal stability in perovskite solar cells. ACS Energy Lett. **3**, 1772 (2018). https://doi.org/10.1021/acsenergylett.8b00926

176. J. Jeong, M. Kim, J. Seo, H. Lu, P. Ahlawat et al., Pseudohalide anion engineering for α-FAPbI₃ perovskite solar cells. Nature **592**, 381–385 (2021). https://doi.org/10.1038/s41586-021-03406-5

177. A. Guerrero, J. You, C. Aranda, Y.S. Kang, G. Garcia-Belmonte et al., Interfacial degradation of planar lead halide perovskite solar cells. ACS Nano **10**, 218 (2016). https://doi.org/10.1021/acsnano.5b03687

178. P. Qin, T. Wu, Z. Wang, L. Xiao, L. Ma et al., Grain boundary and interface passivation with Core-Shell Au@CdS nanospheres for high-efficiency perovskite solar cells. Adv. Funct. Mater. **30**, 1908408 (2020). https://doi.org/10.1002/adfm.201908408

179. A. Davis, T. Tran, D. Young, Solution chemistry of iodide leaching of gold. Hydrometallurgy **32**, 143 (1993). https://doi.org/10.1016/0304-386X(93)90020-E

180. L. Liang, Y. Cai, X. Li, M.K. Nazeeruddin, P. Gao, All that glitters is not gold: recent progress of alternative counter electrodes for perovskite solar cells. Nano Energy **52**, 211 (2018). https://doi.org/10.1016/j.nanoen.2018.07.049

181. M. Kaltenbrunner, G. Adam, E.D. Głowacki, M. Drack, R. Schwödiauer et al., Flexible high power-per-weight perovskite solar cells with chromium oxide–metal contacts for improved stability in air. Nat. Mater. **14**, 1032 (2015). https://doi.org/10.1038/nmat4388

182. S. Cacovich, L. Ciná, F. Matteocci, G. Divitini, P.A. Midgley et al., Gold and iodine diffusion in large area perovskite solar cells under illumination. Nanoscale **9**, 4700 (2017). https://doi.org/10.1039/C7NR00784A

183. K. Domanski, J.-P. Correa-Baena, N. Mine, M.K. Nazeeruddin, A. Abate et al., Not all that glitters is gold: metal-migration-induced degradation in perovskite solar cells. ACS Nano **10**, 6306 (2016). https://doi.org/10.1021/acsnano.6b02613

184. N.N. Shlenskaya, N.A. Belich, M. Grätzel, E.A. Goodilin, A.B. Tarasov, Light-induced reactivity of gold and hybrid perovskite as a new possible degradation mechanism in perovskite solar cells. J. Mater. Chem. A **6**, 1780 (2018). https://doi.org/10.1039/C7TA10217H

185. R.A. Kerner, P. Schulz, J.A. Christians, S.P. Dunfield, B. Dou et al., Reactions at noble metal contacts with methylammonium lead triiodide perovskites: role of underpotential deposition and electrochemistry. APL Mater. **7**, 041103 (2019). https://doi.org/10.1063/1.5083812

186. Y. Xu, Y. Tian, M. Hou, Y. Wu, Y. Ding et al., Performance promotion through dual-interface engineering of CuSCN layers in planar perovskite solar cells. J. Phys. Chem. C **124**, 27977 (2020). https://doi.org/10.1021/acs.jpcc.0c09794

187. Y. Yang, M.T. Hoang, D. Yao, N.D. Pham, V.T. Tiong et al., Spiro-OMeTAD or CuSCN as a preferable hole transport material for carbon-based planar perovskite solar cells. J. Mater. Chem. A **8**, 12723 (2020). https://doi.org/10.1039/D0TA03951A

188. M. Jørgensen, K. Norrman, F.C. Krebs, Stability/degradation of polymer solar cells. Sol. Energy Mater. Sol. Cells **92**, 686 (2008). https://doi.org/10.1016/j.solmat.2008.01.005

189. S. Guo, X. Sun, C. Ding, R. Huang, M. Tan et al., Non-uniform chemical corrosion of metal electrode of p–i–n type of perovskite solar cells caused by the diffusion of CH_3NH_3I. Energy Technol. **8**, 2000250 (2020). https://doi.org/10.1002/ente.202000250

190. L. Zhao, R.A. Kerner, Z. Xiao, Y.L. Lin, K.M. Lee et al., Redox chemistry dominates the degradation and decomposition of metal halide perovskite optoelectronic devices. ACS Energy Lett. **1**, 595 (2016). https://doi.org/10.1021/acsenergylett.6b00320

191. Y.-H. Lin, N. Sakai, P. Da, J. Wu, C. Sansom Harry et al., A piperidinium salt stabilizes efficient metal-halide perovskite solar cells. Science **369**, 96 (2020). https://doi.org/10.1126/science.aba1628

192. M. Kim, S.G. Motti, R. Sorrentino, A. Petrozza, Enhanced solar cell stability by hygroscopic polymer passivation of metal halide perovskite thin film. Energy Environ. Sci. **11**, 2609 (2018). https://doi.org/10.1039/C8EE01101J

193. Q. Wang, Q. Dong, T. Li, A. Gruverman, J. Huang, Thin insulating tunneling contacts for efficient and water-resistant perovskite solar cells. Adv. Mater. **28**, 6734 (2016). https://doi.org/10.1002/adma.201600969

194. Z. Wu, T. Song, B. Sun, Carbon-based materials used for perovskite solar cells. ChemNanoMat **3**, 75 (2017). https://doi.org/10.1002/cnma.201600312

195. L. Gao, I. Spanopoulos, W. Ke, S. Huang, I. Hadar et al., Improved environmental stability and solar cell efficiency of (MA, FA) PbI_3 perovskite using a wide-band-gap 1D thiazolium lead iodide capping layer strategy. ACS Energy Lett. **4**, 1763 (2019). https://doi.org/10.1021/acsenergylett.9b00930

196. Y. Hou, X. Du, S. Scheiner, D.P. McMeekin, Z. Wang et al., A generic interface to reduce the efficiency-stability-cost gap of perovskite solar cells. Science **358**, 1192 (2017). https://doi.org/10.1126/science.aao5561

197. J. Kim, Y. Lee, B. Gil, A.J. Yun, J. Kim et al., A Cu_2O–CuSCN nanocomposite as a hole-transport material of perovskite solar cells for enhanced carrier transport and suppressed interfacial degradation. ACS Appl. Energy Mater. **3**, 7572 (2020). https://doi.org/10.1021/acsaem.0c01001

198. S.S. Mali, J.V. Patil, H. Kim, R. Luque, C.K. Hong, Highly efficient thermally stable perovskite solar cells via $Cs:NiO_x$/CuSCN double-inorganic hole extraction layer interface engineering. Mater. Today **26**, 8 (2019). https://doi.org/10.1016/j.mattod.2019.01.017

199. J. Cao, B. Wu, R. Chen, Y. Wu, Y. Hui et al., Efficient, hysteresis-free, and stable perovskite solar cells with ZnO as electron-transport layer: effect of surface passivation. Adv. Mater. **30**, 1705596 (2018). https://doi.org/10.1002/adma.201705596

200. R. Azmi, C.-L. Lee, I.H. Jung, S.-Y. Jang, Simultaneous improvement in efficiency and stability of low-temperature-processed perovskite solar cells by interfacial control. Adv. Energy Mater. **8**, 1702934 (2018). https://doi.org/10.1002/aenm.201702934

201. W. Qiu, M. Buffière, G. Brammertz, U.W. Paetzold, L. Froyen et al., High efficiency perovskite solar cells using a PCBM/ZnO double electron transport layer and a short air-aging step. Org. Electron. **26**, 30 (2015). https://doi.org/10.1016/j.orgel.2015.06.046

202. S. Zheng, W. Li, T. Su, F. Xie, J. Chen et al., Metal oxide cro_x as a promising bilayer electron transport material for enhancing the performance stability of planar perovskite solar cells. Sol. RRL **2**, 1700245 (2018). https://doi.org/10.1002/solr.201700245

203. Z. Jiang, X. Chen, X. Lin, X. Jia, J. Wang et al., Amazing stable open-circuit voltage in perovskite solar cells using AgAl alloy electrode. Sol. Energy Mater. Sol. Cells **146**, 35 (2016). https://doi.org/10.1016/j.solmat.2015.11.026

204. E. Bi, H. Chen, F. Xie, Y. Wu, W. Chen et al., Diffusion engineering of ions and charge carriers for stable efficient perovskite solar cells. Nat. Commun. **8**, 15330 (2017). https://doi.org/10.1038/ncomms15330

205. J. Lee, S. Singh, S. Kim, S. Baik, Graphene interfacial diffusion barrier between CuSCN and Au layers for stable perovskite solar cells. Carbon **157**, 731 (2020). https://doi.org/10.1016/j.carbon.2019.10.101

206. Q. Jiang, J. Tong, Y. Xian, R.A. Kerner, S.P. Dunfield et al., Surface reaction for efficient and stable inverted perovskite solar cells. Nature **611**, 278 (2022). https://doi.org/10.1038/s41586-022-05268-x

207. X. Li, W. Zhang, X. Guo, C. Lu, J. Wei et al., Constructing heterojunctions by surface sulfidation for efficient inverted perovskite solar cells. Science **375**, 434 (2022). https://doi.org/10.1126/science.abl5676

208. F. Zhang, K. Zhu, Additive engineering for efficient and stable perovskite solar cells. Adv. Energy Mater. **10**, 1902579 (2020). https://doi.org/10.1002/aenm.201902579

209. D. Bi, P. Gao, R. Scopelliti, E. Oveisi, J. Luo et al., High-performance perovskite solar cells with enhanced environmental stability based on amphiphile-modified

CH₃NH₃PbI₃. Adv. Mater. **28**, 2910 (2016). https://doi.org/10.1002/adma.201505255

210. Y. Zhao, J. Wei, H. Li, Y. Yan, W. Zhou et al., A polymer scaffold for self-healing perovskite solar cells. Nat. Commun. **7**, 1 (2016). https://doi.org/10.1038/ncomms10228

211. X. Li, W. Zhang, W. Zhang, H.-Q. Wang, J. Fang, Spontaneous grain polymerization for efficient and stable perovskite solar cells. Nano Energy **58**, 825 (2019). https://doi.org/10.1016/j.nanoen.2019.02.009

212. L. Zuo, H. Guo, D.W. deQuilettes, S. Jariwala, N. deMarco et al., Polymer-modified halide perovskite films for efficient and stable planar heterojunction solar cells. Sci. Adv. **3**, e1700106 (2017)

213. X. Li, W. Zhang, Y.-C. Wang, W. Zhang, H.-Q. Wang et al., In-situ cross-linking strategy for efficient and operationally stable methylammoniun lead iodide solar cells. Nat. Commun. **9**, 1 (2018). https://doi.org/10.1038/s41467-018-06204-2

214. S. Bai, P. Da, C. Li, Z. Wang, Z. Yuan et al., Planar perovskite solar cells with long-term stability using ionic liquid additives. Nature **571**, 245 (2019). https://doi.org/10.1038/s41586-019-1357-2

215. L. Gao, S. Huang, L. Chen, X. Li, B. Ding et al., Excellent stability of perovskite solar cells by passivation engineering. Sol. RRL **2**, 1800088 (2018). https://doi.org/10.1002/solr.201800088

216. G.Y. Kim, A. Senocrate, T.-Y. Yang, G. Gregori, M. Grätzel et al., Large tunable photoeffect on ion conduction in halide perovskites and implications for photodecomposition. Nat. Mater. **17**, 445 (2018). https://doi.org/10.1038/s41563-018-0038-0

217. Q. Lou, H. Li, Q. Huang, Z. Shen, F. Li et al., Multifunctional CNT: TiO₂ additives in spiro-OMeTAD layer for highly efficient and stable perovskite solar cells. EcoMat **3**, e12099 (2021). https://doi.org/10.1002/eom2.12099

218. Q. Luo, Y. Zhang, C. Liu, J. Li, N. Wang et al., Iodide-reduced graphene oxide with dopant-free spiro-OMeTAD for ambient stable and high-efficiency perovskite solar cells. J. Mater. Chem. A **3**, 15996 (2015). https://doi.org/10.1039/C5TA02710A

219. Y. Han, G. Zhang, H. Xie, T. Kong, Y. Li et al., Azide additive acting as a powerful locker for Li⁺ and TBP in spiro-OMeTAD toward highly efficient and stable perovskite solar cells. Nano Energy (2022). https://doi.org/10.1016/j.nanoen.2022.107072

220. Y. Shao, Y. Fang, T. Li, Q. Wang, Q. Dong et al., Grain boundary dominated ion migration in polycrystalline organic–inorganic halide perovskite films. Energy Environ. Sci. **9**, 1752 (2016). https://doi.org/10.1039/C6EE00413J

221. R. Wang, J. Xue, L. Meng, J.-W. Lee, Z. Zhao et al., Caffeine improves the performance and thermal stability of perovskite solar cells. Joule **3**, 1464 (2019). https://doi.org/10.1016/j.joule.2019.04.005

222. L. Liu, S. Huang, Y. Lu, P. Liu, Y. Zhao et al., Grain-boundary "patches" by in situ conversion to enhance perovskite solar cells stability. Adv. Mater. **30**, 1800544 (2018). https://doi.org/10.1002/adma.201800544

223. X. Li, S. Ke, X. Feng, X. Zhao, W. Zhang et al., Enhancing the stability of perovskite solar cells through cross-linkable and hydrogen bonding multifunctional additives. J. Mater. Chem. A **9**, 12684 (2021). https://doi.org/10.1039/D1TA01572A

224. Y. Ma, Y. Cheng, X. Xu, M. Li, C. Zhang et al., Suppressing ion migration across perovskite grain boundaries by polymer additives. Adv. Funct. Mater. **31**, 2006802 (2021). https://doi.org/10.1002/adfm.202006802